Synthesis, Crystal Structures, Mössbauer, Susceptibility, and EPR Studies of a Series of Spin Exchange Coupled Complexes Containing the (μ-Oxo)bis(μ-acetato)rutheniummetal Core and Its Hydroxo-Bridged Analogue (Metal = V, Cr, Mn, Fe, Co)

Rainer Hotzelmann,[1a] Karl Wieghardt,*[,1a] Jürgen Ensling,[1b] Harald Romstedt,[1b] Philipp Gütlich,[1b] Eckhard Bill,[1c] Ulrich Flörke,[1d] and Hans-Jürgen Haupt[1d]

Contribution from the Lehrstuhl für Anorganische Chemie I, Ruhr-Universität, D-4630 Bochum, Germany, the Institut für Anorganische und Analytische Chemie, Johannes-Gutenberg-Universität, D-6500 Mainz, Germany, the Lehrstuhl für Allgemeine Anorganische und Analytische Chemie der Universität-Gesamthochschule, D-4790 Paderborn, Germany, and the Institut für Physik der Medizinischen Universität, D-2400 Lübeck, Germany.
Received June 1, 1992

Abstract: Co hydrolysis of equimolar amounts of the mononuclear complexes L'RuCl$_3$·H$_2$O and LMCl$_3$ (M = Co^{III}, V^{III}, Mn^{III}, Fe^{III}) in methanol solutions which contain an excess of sodium acetate affords the asymmetric, heterodinuclear complexes [L'Ru(μ-O)(μ-CH$_3$CO$_2$)$_2$ML]$^{2+}$ (M = Co (**1**), V (**2**), Mn (**4**), Fe (**5**)) which have been isolated as crystalline bis(hexafluorophosphate) salts by addition of NaPF$_6$. The same reaction using L'CrBr$_3$ and LRuCl$_3$ yields [LRu(μ-O)(μ-CH$_3$CO$_2$)$_2$CrL'](PF$_6$)$_2$ (**3**) (L = 1,4,7-triazacyclononane, C$_6$H$_{15}$N$_3$; L' = 1,4,7-trimethyl-1,4,7-triazacyclononane, C$_9$H$_{21}$N$_3$). Complexes **1**–**5** are electrochemically reversibly oxidized by one electron. Chemically, the oxidized species [L'Ru(μ-O)(μ-CH$_3$CO$_2$)$_2$ML](PF$_6$)$_3$ (M = Mn (**6**), Fe (**7**)) have been generated by oxidation of **4** and **5** in H$_2$O with Na$_2$S$_2$O$_8$. The oxo bridges in **1**, **3**, and **5** are protonated reversibly in acidic solution and the μ-hydroxo complexes [L'Ru(μ-OH)(μ-CH$_3$CO$_2$)$_2$ML](PF$_6$)$_3$ (M = Co (**8**), Fe (**10**)) and [LRu(μ-OH)(μ-CH$_3$CO$_2$)$_2$CrL'](PF$_6$)$_3$ (**9**) have been isolated. The acidic dissociation constants have been determined spectrophotometrically in aqueous solution at 20 °C (pK$_a$ values: (**8**) 8.0, (**9**) 7.5, (**10**) 4.0). The crystal structures of **4**, **8**, the bisperchlorate hexafluorophosphate salt of **6**, and the trisperchlorate monohydrate salt of **7** have been determined by X-ray crystallography: **4**, orthorhombic, *Pbca*, a = 18.985 (4) Å, b = 14.311 (3) Å, c = 24.511 (3) Å, Z = 8; (**6**)(ClO$_4$)$_2$(PF$_6$), monoclinic $P2_1/m$, a = 11.483 (2) Å, b = 9.754 (2) Å, c = 16.307 (4) Å, β = 110.30 (1)°, Z = 2; (**7**)(ClO$_4$)$_3$·H$_2$O, monoclinic $P2_1/m$, a = 11.472 (3) Å, b = 9.752 (2) Å, c = 16.623 (2) Å, β = 110.33 (1)°, Z = 2; **8**, monoclinic $P2_1/m$, a = 11.986 (3) Å, b = 10.010 (2) Å, c = 16.383 (4) Å, β = 111.20 (1)°, Z = 2. Complexes **4**, **6**, and **7** contain a (μ-oxo)bis(μ-acetato)rutheniummetal core where the Ru ions are capped by the tridentate macrocycle L' and the first-row transition metals by L; **8** contains a μ-hydroxo bridge. From temperature-dependent (4–295 K) susceptibility measurements on powdered samples of **1**–**8** nearly temperature-independent magnetic moments have been calculated which indicate the following electronic ground states: (**1**), $S = {}^1/_2$; (**2**), $S = {}^1/_2$; (**3**), S = 1; (**4**), $S = {}^3/_2$; (**5**), S = 2; (**6**) S = 1; (**7**), $S = {}^3/_2$; (**8**), $S = {}^1/_2$. Low-temperature EPR measurements confirm these electronic states. The μ-hydroxo species **9** and **10** have temperature-dependent magnetic moments; weak antiferromagnetic spin exchange coupling has been observed. The assignment of oxidation states in these heterodinuclear complexes proved to be not trivial. Mössbauer spectra of **5**, **7**, and **10** indicate the presence of an octahedral high-spin ferric ion in each case. **5** is therefore formulated as [Ru^{III}OFe^{III}]$^{2+}$, **7** as [Ru^{IV}OFe^{III}]$^{3+}$, and **10** as [Ru^{III}(OH)Fe^{III}]$^{3+}$. From the combined physical data the oxidation states in the other complexes are assigned: (**1**) [Ru^{III}OCo^{III}]$^{2+}$; (**2**) [Ru^{III}OV^{IV}]$^{2+}$, (**3**) [Ru^{III}OCr^{III}]$^{2+}$, (**4**) [Ru^{III}OMn^{III}]$^{2+}$, (**6**) [Ru^{III}OMn^{IV}]$^{3+}$, (**8**) [Ru^{III}(OH)Co^{III}]$^{3+}$, and (**9**) [Ru^{III}(OH)Cr^{III}]$^{3+}$. A model to interpret the very strong spin exchange coupling in complexes **2**–**7** is presented.

Introduction

The (μ-oxo)bis(μ-carboxylato)dimetal core (Chart I) is a ubiquitous structural motif in biology and inorganic chemistry. Iron[2] and manganese[3] containing metalloproteins of which the active sites consist of this structural entity have been characterized by spectroscopic methods and X-ray crystallography. Subsequently, a rapidly growing number of low molecular weight, dinuclear complexes with first-row transition-metal ions, e.g. Ti^{III},[4] V^{III},[5] Cr^{III},[6] Mn^{III},[7] and Fe^{III},[8] have been synthesized. Their

Chart I

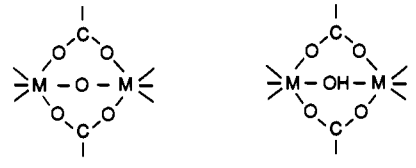

I II

M: Ti, V, Cr, Mn, Fe, Mo, Ru, Os

V, Cr, Fe, Co, Ni, Mo, Ru

(1) (a) Ruhr-Universität. (b) Universität Mainz. (c) Medizinische Universität Lübeck. (d) Universität-Gesamthochschule Paderborn.

(2) Recent reviews on non-heme iron metalloproteins and model μ-oxo complexes: (a) Lippard, S. J. *Angew. Chem., Int. Ed. Engl.* **1988**, *27*, 344. (b) Vincent, J. B.; Olivier-Lilley, G. L.; Averill, B. A. *Chem. Rev.* **1990**, *90*, 1447. (c) Que, L., Jr.; True, A. E. *Progr. Inorg. Chem.* **1990**, *38*, 97. (d) Kurtz, D. M., Jr. *Chem. Rev.* **1990**, *90*, 585. (e) Wilkins, P. C.; Wilkins, R. G. *Coord. Chem. Rev.* **1987**, *79*, 195. (f) Klotz, I. M.; Kurtz, D. M., Jr. *Acc. Chem. Res.* **1984**, *17*, 16–22. (g) Sanders-Loehr, J. *Iron Carriers and Iron Proteins*; Loehr, T. M., Ed.; VCH: Weinheim, 1989; p 373. (h) Que, L., Jr.; Scarrow, R. C. *Metal Clusters in Proteins*; Que, L., Jr., Ed.; ACS Symp. Ser. No. 372; American Chemical Society: Washington, DC, 1988; p 152.

(3) Recent reviews on manganese-containing metalloproteins and model μ-oxo complexes: (a) Wieghardt, K. *Angew. Chem., Int. Ed. Engl.* **1989**, *28*, 1153. (b) Pecoraro, V. L. *Photochem. Photobiol.* **1988**, *48*, 249. (c) Christou, G.; Vincent, J. B. *Metal Cluster in Proteins*; ACS Symp. Ser. No. 372; Que, L., Jr., Ed.; American Chemical Society: Washington, DC, 1988; p 239. (d) Brudvig, G. W.; Crabtree, R. H. *Prog. Inorg. Chem.* **1989**, *37*, 99. (e) Vincent, J. B.; Christou, G. *Adv. Inorg. Chem.* **1989**, *33*, 197. (f) Christou, G. *Acc. Chem. Res.* **1989**, *22*, 328. (g) Christou, G.; Vincent, J. B. *Metal Clusters in Proteins*; Que, L., Jr., Ed.; ACS Symp. Ser. No. 372; American Chemical Society: Washington, DC, 1988; p 238.

(4) Bodner, A.; Drüeke, S.; Wieghardt, K.; Nuber, B.; Weiss, J. *Angew. Chem., Int. Ed. Engl.* **1990**, *29*, 68.

0002-7863/92/1514-9470$03.00/0

Chart II

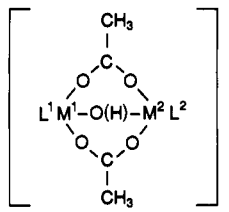

symmetric homodinuclear: $M^1{=}M^2$; $L^1{=}L^2$
asymmetric homodinuclear: $M^1{=}M^2$; $L^1{\neq}L^2$
symmetric heterodinuclear: $M^1{\neq}M^2$; $L^1{=}L^2$
asymmetric heterodinuclear: $M^1{\neq}M^2$; $L^1{\neq}L^2$

structures have been determined, and their electronic and magnetic properties have been studied in detail. The metal ions are, in general, in an octahedral ligand environment with coordinated, tridentate capping ligands such as hydrotris(pyrazolyl)borate ($HBpz_3^-$), 1,4,7-triazacyclononane (L), and 1,4,7-trimethyl-1,4,7-triazacyclononane (L') completing the coordination spheres (N_3O_3 donor set).

It was discovered that the μ-oxo species display very diverse spin exchange coupling phenomena. The unpaired electrons at the two first-row transition-metal ions are—depending on their d^n electron configuration—either intramolecularly antiferromagnetically or ferromagnetically coupled by a superexchange mechanism. In a recent publication[9] we have analyzed the magnetic properties of these symmetric *homo*dinuclear and a series of asymmetric *hetero*dinuclear complexes with differing d^m and d^n electronic configurations of the metal ions. This enabled us to identify the relevant magnetic orbitals which mediate the spin exchange coupling.

In this paper we label such a dinuclear species *symmetric* when the capping ligands are the same at both metal ions (which are identical in *homo*dinuclear or not in *hetero*dinuclear complexes) and *asymmetric* (homo- or heterodinuclear) when the two capping ligands per dinuclear unit are different (Chart II). If the nature of the capping ligands is irrelevant, we will use the short-hand notation $[M^1OM^2]^{n+}$ and $[M^1(OH)M^2]^{n+}$ for μ-oxo and μ-hydroxo complexes, respectively.

Core structures I and II have also been identified in a few second- and third-row transition-metal homodinuclear complexes: Mo^{III},[10] Ru^{III},[11] Os^{IV}.[12] Since the M···M distances in μ-oxo complexes of first-row transition-metal ions vary in the narrow range between ~3.1 and ~3.25 Å, direct metal–metal bonding has been ruled out. The situation is not so simple for the heavier transition-metal analogues. In diamagnetic $[L'_2Mo_2^{III}(\mu\text{-}O)(\mu\text{-}CH_3CO_2)_2]^{2+}$ the short Mo–Mo distance of 2.885 (1) Å is clear evidence for the presence of a Mo–Mo multiple bond (Mo≡Mo). Upon protonation, yielding antiferromagnetically coupled $[L'_2Mo_2^{III}(\mu\text{-}OH)(\mu\text{-}CH_3CO_2)_2]^{3+}$, the Mo···Mo distance increases dramatically to 3.555 (1) Å, indicating thereby the absence of metal–metal bonding.[10] It is now well established that protonation of μ-oxo and/or μ-hydroxo species always results in a significant lengthening of the $M\text{–}O_{bridge}$ distances and, as a consequence, the M···M distances increase by ~0.2 Å per protonation step provided that no metal–metal bonding prevails in the protonated or unprotonated species.

In diamagnetic $[L'_2Ru_2^{III}(\mu\text{-}O)(\mu\text{-}CH_3CO_2)_2]^{2+}$ and its protonated, antiferromagnetically coupled analogue $[L'_2Ru_2^{III}(\mu\text{-}OH)(\mu\text{-}CH_3CO_2)_2]^{3+}$ the Ru···Ru distances are at 3.258 (1) Å and 3.472 (2) Å, respectively.[11a] The former may or may not have a weak direct Ru···Ru interaction (single bond?) which is not present in the latter. In the $[Os_2^{IV}(\mu\text{-}O)(\mu\text{-}CH_3CO_2)_2]^{4+}$ core the Os···Os distance of 3.440 (2) Å excludes direct metal–metal bonding;[12] it reflects electrostatic repulsion between the highly charged Os^{IV} ions. The observed diamagnetism of $[Ru^{III}ORu^{III}]^{2+}$ and $[Os^{IV}OOs^{IV}]^{4+}$ species is then due to strong antiferromagnetic spin exchange coupling via a superexchange mechanism. All (μ-oxo)diruthenium(III) complexes known to date have an $S = 0$ electronic ground state. Meyer et al.[13] have used simple molecular orbital (MO) considerations which were originally introduced by Dunitz and Orgel[14] for diamagnetic $[Cl_5Ru^{IV}(\mu\text{-}O)Ru^{IV}Cl_5]^{4-}$ to explain the bonding in corner sharing μ-oxo bridged octahedral second- (and third-) row transition-metal complexes. In first-row transition-metal complexes of this type the MO description is more complicated because the energy of $2p_x$, $2p_y$, $2p_z$ orbitals of the oxo ligand is much lower than the energy of 3d metal orbitals. Consequently, a description using localized metal orbitals is more appropriate, where the oxo ligand orbitals participate only as perturbations on the metal orbitals.[9]

We decided that it would be interesting to study the electronic and magnetic properties of a series of heterodinuclear μ-oxo and μ-hydroxo complexes where one of the metal ions is always ruthenium and the other one is a first-row transition-metal ion (V, Cr, Mn, Fe, Co).[15] We have succeeded in synthesizing a series of such asymmetric heterodinuclear complexes (Scheme I).

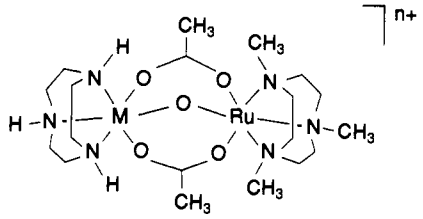

We present here the first study of such structurally very similar heterodinuclear (μ-oxo)rutheniummetal complexes which have been characterized by X-ray crystallography, ESR, Mössbauer,

(5) (a) Knopp, P.; Wieghardt, K. *Inorg. Chem.* **1991**, *30*, 4061. (b) Wieghardt, K.; Köppen, M.; Nuber, B.; Weiss, J. *J. Chem. Soc., Chem. Commun.* **1986**, 1530. (c) Köppen, M.; Fresen, G.; Wieghardt, K.; Llusar, R. M.; Nuber, B.; Weiss, J. *Inorg. Chem.* **1988**, *27*, 721. (d) Knopp, P.; Wieghardt, K.; Nuber, B.; Weiss, J.; Sheldrick, W. S. *Inorg. Chem.* **1990**, *29*, 363.

(6) Martin, L. L.; Wieghardt, K.; Blondin, G.; Girerd, J.-J.; Nuber, B.; Weiss, J. *J. Chem. Soc., Chem. Commun.* **1990**, 1767.

(7) (a) Wieghardt, K.; Bossek, U.; Ventur, D.; Weiss, J. *J. Chem. Soc., Chem. Commun.* **1985**, 347. (b) Bossek, U.; Wieghardt, K.; Nuber, B.; Weiss, J. *Inorg. Chim. Acta* **1989**, *165*, 123. (c) Sheats, J. E.; Czernuszewicz, R. S.; Dismukes, G. C.; Rheingold, A.; Petrouleas, V.; Stubbe, J.; Armstrong, W. H.; Beer, R. H.; Lippard, S. J. *J. Am. Chem. Soc.* **1987**, *109*, 1435. (d) Wieghardt, K.; Bossek, U.; Nuber, B.; Weiss, J.; Bonvoisin, J.; Corbella, M.; Vitols, S. E.; Girerd, J. J. *J. Am. Chem. Soc.* **1988**, *110*, 7398. (e) Ménage, S.; Girerd, J.-J.; Gleizes, A. *J. Chem. Soc., Chem. Commun.* **1988**, 431. (f) Vincent, J. B.; Folting, K.; Huffmann, J. C.; Christou, G. *Biochem. Soc. Trans.* **1988**, *16*, 822. (g) Feng-Jung, W.; Kurtz, D. M., Jr.; Hagen, K. S.; Nymann, P. D.; Debrunner, P. G.; Vankai, V. A. *Inorg. Chem.* **1990**, *29*, 5174. (h) Toftlund, H.; Markiewicz; Murray, K. S. *Acta Chem. Scand.* **1990**, *44*, 443.

(8) (a) Armstrong, W. H.; Lippard, S. J. *J. Am. Chem. Soc.* **1983**, *105*, 4837. (b) Wieghardt, K.; Pohl, K.; Gebert, W. *Angew. Chem., Int. Ed. Engl.* **1983**, *22*, 727. (c) Hartman, J.; Rardin, R. L.; Chaudhuri, P.; Pohl, K.; Wieghardt, K.; Nuber, B.; Weiss, J.; Papaefthymiou, G. C.; Frankel, R. B.; Lippard, S. J. *J. Am. Chem. Soc.* **1987**, *109*, 7397. (d) Armstrong, W. H.; Spool, A.; Papaefthymiou, G. C.; Frankel, R. B.; Lippard, S. J. *J. Am. Chem. Soc.* **1984**, *106*, 3653. (e) Toftlund, H.; Murray, K. S.; Zwack, P. R.; Taylor, L. F.; Anderson, O. P. *J. Chem. Soc., Chem. Commun.* **1986**, 191.

(9) Hotzelmann, R.; Wieghardt, K.; Flörke, U.; Haupt, H.-J.; Weatherburn, D. C.; Bonvoisin, J.; Blondin, G.; Girerd, J.-J. *J. Am. Chem. Soc.* **1992**, *114*, 1681.

(10) Wieghardt, K.; Bossek, U.; Neves, A.; Nuber, B.; Weiss, J. *Inorg. Chem.* **1989**, *28*, 432.

(11) (a) Neubold, P.; Wieghardt, K.; Nuber, B.; Weiss, J. *Inorg. Chem.* **1989**, *28*, 459. (b) Sasaki, Y.; Suzuki, M.; Tokiwa, A.; Ebihara, M.; Yamaguchi, T.; Kabuto, C.; Ito, T. *J. Am. Chem. Soc.* **1988**, *110*, 6251. (c) Llobet, A.; Curry, M. E.; Evans, H. T.; Meyer, T. J. *Inorg. Chem.* **1989**, *28*, 3131. (d) Das, B. K.; Chakravarty, A. R. *Inorg. Chem.* **1990**, *29*, 2078. (e) Das, B. K.; Chakravarty, A. R. *Inorg. Chem.* **1991**, *30*, 4978.

(12) Armstrong, J. W.; Robinson, W. R.; Walton, R. A. *Inorg. Chem.* **1983**, *22*, 1301.

(13) Weaver, T. R.; Meyer, T. J.; Adeyemi, S. A.; Brown, G. M.; Eckberg, R. P.; Hatfield, W. E.; Johnson, E. C.; Murray, R. W.; Unterecker, D. *J. Am. Chem. Soc.* **1975**, *97*, 3039.

(14) Dunitz, J. D.; Orgel, L. E. *Chem. Soc. London* **1953**, 2595.

(15) Hotzelmann, R.; Wieghardt, K.; Flörke, U.; Haupt, H.-J. *Angew. Chem., Int. Ed. Engl.* **1990**, *29*, 645.

and UV–vis spectroscopy, and magnetic susceptibility measurements.

Experimental Section

The ligand 1,4,7-triazacyclononane (L) and its methylated derivative 1,4,7-trimethyl-1,4,7-triazacyclononane (L') were prepared according to published procedures.[16] The precursor complexes $LCoCl_3$,[16a] $LFeCl_3$,[18] $LRuCl_3$,[17] $L'RuCl_3{\cdot}H_2O$,[11a] $L'CrBr_3$,[19] and $[L_2Mn_2(\mu\text{-}O)(\mu\text{-}CH_3CO_2)_2](PF_6)_2$[7a] were also prepared as described previously.

Elemental analyses (C, H, N) were performed in the microanalytical laboratory of the Ruhr-Universität Bochum. The first-row transition-metal content of heterodinuclear complexes was determined spectrophotometrically according to Hartkamp's procedures:[20] Co^{III}, Fe^{III}, Mn^{III} as bis(pyridine-2,6-dicarboxylato)metal(III) complexes, V as $[VO(dipic)(O_2)]^-$, and Cr as CrO_4^{2-}.

Preparation of Complexes. (a) $LVCl_3$. To a deoxygenated solution of VCl_3 (1.0 g, 6.4 mmol) in dry dimethylformamide (dmf) (50 mL) was added 1,4,7-triazacyclononane (L) (0.82 g, 6.4 mmol). After the solution was heated to reflux for 1 h and cooled to room temperature a green microcrystalline precipitate formed which was collected by filtration, washed with diethyl ether, and air dried. Yield: 0.42 g (23%). Anal. Calcd for $C_6H_{15}N_3Cl_3V$: C, 25.2; H, 5.2; N, 14.7; Cl, 37.1. Found: C, 25.5; H, 5.4; N, 14.6; Cl, 37.0.

(b) $[L'Ru(\mu\text{-}O)(\mu\text{-}CH_3CO_2)_2CoL](PF_6)_2$ (1). A suspension of sodium acetate (1.0 g), $L'RuCl_3{\cdot}H_2O$ (0.16 g, 0.40 mmol), and $LCoCl_3$ (0.12 g, 0.40 mmol) in methanol (40 mL) was heated to reflux for 90 min. To the then deep-green solution were added a few drops of a 1.0 M sodium methanolate solution and $NaPF_6$ (0.80 g). Upon cooling to 10 °C green-black crystals of 1 precipitated and were collected by filtration, washed with ethanol and ether, and air dried (0.14 g, 38%). Anal. Calcd for $[C_{19}H_{42}CoN_6O_5Ru](PF_6)_2$: C, 25.8; H, 4.8; N, 9.5; Co, 6.7. Found: C, 25.6; H, 4.7; N, 9.3; Co, 6.7.

(c) $[L'Ru(\mu\text{-}O)(\mu\text{-}CH_3CO_2)_2VL](PF_6)_2$ (2). An argon purged suspension of $L'RuCl_3{\cdot}H_2O$ (0.15 g, 0.38 mmol), $LVCl_3$ (0.11 g, 0.38 mmol), and sodium acetate (0.50 g) in methanol (40 mL) was heated to reflux for 1 h under an argon blanketing atmosphere. To the deep-blue, clear solution was added $NaPF_6$ (0.80 g). Upon cooling to −18 °C blue-black crystals of 2 precipitated (0.12 g, 36%) within 2–3 days, which were collected by filtration, washed with ethanol and ether, and air dried. Anal. Calcd for $[C_{19}H_{42}N_6O_5RuV](PF_6)_2$: C, 26.0; H, 4.8; N, 9.6. Found: C, 25.8; H, 4.5; N, 9.4.

(d) $[LRu(\mu\text{-}O)(\mu\text{-}CH_3CO_2)_2CrL'](PF_6)_2$ (3). This complex was prepared as described for 2 by using $L'CrBr_3$ (0.17 g, 0.37 mmol), $LRuCl_3$ (0.13 g, 0.37 mmol), and sodium acetate (1.2 g) as starting materials. After refluxing for 90 min a solution of $NaPF_6$ (0.80 g) in methanol (10 mL) to which a small amount of sodium methanolate (0.1 g) had been added was added. Black-brown crystals of 3 were obtained (0.13 g, 40%). Anal. Calcd for $[C_{19}H_{42}CrN_6O_5Ru](PF_6)_2$: C, 26.0; H, 4.8; N, 9.6; Cr, 5.9. Found: C, 26.1; H, 5.0; N, 9.3; Cr, 5.7.

(e) $[L'Ru(\mu\text{-}O)(\mu\text{-}CH_3CO_2)_2MnL](PF_6)_2$ (4). A solution of sodium acetate (0.5 g), $L'RuCl_3{\cdot}H_2O$ (0.15 g, 0.38 mmol), and $[L_2Mn_2(\mu\text{-}O)(\mu\text{-}CH_3CO_2)_2](PF_6)_2$ (0.15 g, 0.19 mmol) in methanol (40 mL) was heated to reflux for 1 h. Upon addition of $NaPF_6$ (0.8 g) to the green solution and cooling to 0 °C dark green crystals of 4 precipitated within 2–3 days (0.17 g, 51%). Anal. Calcd for $[C_{19}H_{42}MnN_6O_5Ru](PF_6)_2$: C, 25.9; H, 4.8; N, 9.5; Mn, 6.2. Found: C, 25.8; H, 5.0; N, 9.4; Mn, 6.3.

(f) $[L'Ru(\mu\text{-}O)(\mu\text{-}CH_3CO_2)_2FeL](PF_6)_2$ (5). This complex was prepared as described for 1 by using $L'RuCl_3{\cdot}H_2O$ (0.15 g, 0.38 mmol), $LFeCl_3$ (0.11 g, 0.38 mmol), and sodium acetate (0.5 g) as starting materials. Dark-red crystals of 5 were obtained (0.15 g, 45%). Anal. Calcd for $[C_{19}H_{42}FeN_6O_5Ru](PF_6)_2$: C, 25.9; H, 4.8; N, 9.5; Fe, 6.3. Found: C, 25.8; H, 4.9; N, 9.5; Fe, 6.5.

(g) $[L'Ru(\mu\text{-}O)(\mu\text{-}CH_3CO_2)_2MnL](PF_6)_3$ (6). To an aqueous solution (30 mL) of 4 (0.26 g, 0.30 mmol) was added $Na_2S_2O_8$ (0.25 g). After the green solution was stirred for 10 min at ambient temperature $NaPF_6$ (0.51 g) was added. Dark green microcrystals of 6 precipitated immediately and were collected by filtration, washed with ethanol and ether, and air dried (0.20 g, 65%). Anal. Calcd for $[C_{19}H_{42}MnN_6O_5Ru](PF_6)_3$: C, 21.9; H, 4.3; N, 8.1; Mn, 5.3. Found: C, 21.9; H, 4.1; N, 7.9; Mn, 5.5.

(h) $[L'Ru(\mu\text{-}O)(\mu\text{-}CH_3CO_2)_2FeL](PF_6)_3$ (7). To an aqueous solution (20 mL) of 5 (0.20 g, 0.23 mmol) was added $Na_2S_2O_8$ (0.20 g). After the solution was stirred for 10 min at ambient temperature and $NaPF_6$ (0.40 g) was added a brown-purple precipitate of 7 was obtained (0.14 g, 59%). Anal. Calcd for $[C_{19}H_{42}FeN_6O_5Ru](PF_6)_3$: C, 22.2; H, 4.1; N, 8.2; Fe, 5.4. Found: C, 22.0; H, 4.2; N, 7.9; Fe, 5.6.

(i) $[L'Ru(\mu\text{-}OH)(\mu\text{-}CH_3CO_2)_2CoL](PF_6)_3$ (8). An argon purged solution of sodium acetate (1.0 g), $L'RuCl_3{\cdot}H_2O$ (0.16 g, 0.40 mmol), and $LCoCl_3$ (0.12 g, 0.40 mmol) in methanol (40 mL) was heated to reflux for 90 min whereupon a clear dark-green solution was obtained. Addition of a few drops of HPF_6 and $NaPF_6$ (0.80 g) and cooling to 0 °C produced red, needle-shaped crystals of 8 (0.17 g, 41%). Alternatively, 8 was obtained in quantitative yield from an aqueous solution of 1 to which HPF_6 and $NaPF_6$ were added. Anal. Calcd for $[C_{19}H_{43}CoN_6O_5Ru](PF_6)_3$: C, 22.1; H, 4.2; N, 8.2; Co, 5.7. Found: C, 21.9; H, 4.1; N, 8.1; Co, 5.7.

(j) $[LRu(\mu\text{-}OH)(\mu\text{-}CH_3CO_2)_2CrL'](PF_6)_3$ (9). To a brown solution of 3 (0.12 g, 0.14 mmol) in methanol (20 mL) were added a few drops of 60% aqueous HPF_6 whereupon an orange microcrystalline solid of 9 precipitated out (0.11 g, 77%). Anal. Calcd for $[C_{19}H_{43}CrN_6O_5Ru](PF_6)_3$: C, 22.3; H, 4.2; N, 8.2. Found: C, 22.0; H, 4.2; N, 8.2.

(k) $[L'Ru(\mu\text{-}OH)(\mu\text{-}CH_3CO_2)_2FeL](PF_6)_3$ (10). To a methanolic solution (30 mL) of 5 (0.18 g, 0.20 mmol) were added a few drops of aqueous 60% HPF_6 whereupon a microcrystalline solid formed which was collected by filtration, washed with dry ether, and air dried (0.19 g, 89%). Anal. Calcd for $[C_{19}H_{43}FeN_6O_5Ru](PF_6)_3$: C, 22.2; H, 4.2; N, 8.2; Fe, 5.4. Found: C, 21.8; H, 4.1; N, 8.0; Fe, 5.6.

Physical Measurements. Infrared spectra of solid samples (KBr disks) were recorded on a Perkin-Elmer FT-IR spectrometer 1720X in the range 4000–400 cm^{-1}. Electronic spectra of complexes dissolved in acetonitrile or aqueous buffer solutions were measured on a Perkin-Elmer Lambda 9 UV/VIS/NIR spectrophotometer in the range 200–1500 nm. X-band EPR spectra were recorded on a Bruker ER 200D X-band spectrometer equipped with a standard TE 102 resonator (ER 4102, Bruker), a helium flow cryostat (ESR 910, Oxford Instruments), a NMR gaussmeter (Bruker B-NM12), a frequency counter (Systron & Donner 6054D), and a data acquisition system (local development, Lübeck). The EPR spectra were recorded with modulation frequency of 100 kHz and modulation amplitude of 1 mT, throughout. For evaluation of parameters the spectra were simulated with a non-quantum-mechanical routine for effective spin $S = {}^1/_2$, using effective g values, hyperfine coupling constants, and angular dependent line widths. Mössbauer spectra have been recorded in the temperature range 5–290 K with a conventional Mössbauer spectrometer operating in a constant acceleration mode and equipped with a $^{57}Co/Rh$ source at room temperature. The sample was placed in a helium flow cryostat (Oxford Instruments Mod CF 506). Measurements of the magnetic susceptibility of complexes were performed on powdered samples in the temperature range ca. 4–295 K on a Foner type magnetometer equipped with a helium flow cryostat. The magnetometer was calibrated with $Hg[Co(NCS)_4]$ at a field of 1 T. Corrections for diamagnetism were carried out by using tabulated Pascal's constants.[21] The apparatus used for recording cyclic voltammograms has been described elsewhere.[5c] A standard three-electrode arrangement (Pt-button or glassy carbon working electrode, Pt-wire auxilliary electrode, Ag/AgCl (saturated LiCl in ethanol) reference electrode) was used. Complexes ($\sim 10^{-3}$ M) were dissolved in acetonitrile with 0.10 M tetra-*n*-butylammonium hexafluorophosphate supporting electrolyte. Under our conditions the redox potential for the ferrocenium/ferrocene couple was found to be +0.53 V vs Ag/AgCl which may be converted to 0.40 V vs NHE.[23]

X-ray Structure Determinations. Dark green crystals of the bishexafluorophosphate salt of 4 were obtained directly from the methanolic reaction solution (see above). Dark green single crystals of $[L'Ru(\mu\text{-}O)(\mu\text{-}CH_3CO_2)_2MnL](ClO_4)_2(PF_6)$ were obtained by slow evaporation at ambient temperature of an acetonitrile/water (1:1) solution containing $NaClO_4$ and the trishexafluorophosphate salt (6). Brownish purple single crystals of the trisperchlorate monohydrate salt $[L'Ru(\mu\text{-}O)(\mu\text{-}CH_3CO_2)_2FeL](ClO_4)_3{\cdot}H_2O$ were obtained by addition of $NaClO_4$ in-

(16) (a) Wieghardt, K.; Schmidt, W.; Nuber, B.; Weiss, J. *Chem. Ber.* **1979**, *112*, 2220. (b) Wieghardt, K.; Chaudhuri, P.; Nuber, B.; Weiss, J. *Inorg. Chem.* **1982**, *21*, 3086.

(17) Wieghardt, K.; Herrmann, W.; Köppen, M.; Jibril, I.; Huttner, G. *Z. Naturforsch.* **1984**, *39b*, 1335.

(18) Wieghardt, K.; Pohl, K.; Gebert, W. *Angew. Chem., Int. Ed. Engl.* **1983**, *22*, 727.

(19) Chaudhuri, P.; Winter, M.; Küppers, H. J.; Wieghardt, K.; Nuber, B.; Weiss, J. *Inorg. Chem.* **1987**, *26*, 3302.

(20) (a) Mn: Hartkamp, H. *Z. Anal. Chem.* **1964**, *199*, 183. (b) Fe: Hartkamp, H. *Z. Anal. Chem.* **1962**, *190*, 66. (c) V: Hartkamp, H. *Z. Anal. Chem.* **1959/1960**, *171*, 262. (d) Co: Hartkamp, H. *Z. Anal. Chem.* **1961**, *182*, 259.

(21) Earnshaw, A. *Introduction to Magnetochemistry*; Academic Press: New York, 1968.

(22) (a) Koepp, H. M.; Wendt, H.; Strehlow, H. *Z. Elektrochem.* **1960**, *64*, 483. (b) Gagné, R. R.; Koval, C. A.; Lisensky, G. C. *Inorg. Chem.* **1980**, *19*, 2855.

(23) *International Tables of Crystallography*; Kynoch: Birmingham, England, **1974**; Vol. IV, pp 99 and 149.

Table I. Crystallographic Data of Complexes

	4	6	7	8
empirical formula	$[C_{19}H_{42}MnN_6O_5Ru](PF_6)_2$	$[C_{19}H_{42}MnN_6O_5Ru](ClO_4)_2(PF_6)$	$[C_{19}H_{42}FeN_6O_5Ru](ClO_4)_3\cdot H_2O$	$[C_{19}H_{43}CoN_6O_5Ru](PF_6)_3$
formula weight	880.5	934.4	925.9	1030.5
space group	*Pbca*	$P2_1/m$	$P2_1/m$	$P2_1/m$
a, Å	18.985 (4)	11.483 (2)	11.472 (3)	11.986 (3)
b, Å	14.311 (3)	9.754 (2)	9.752 (2)	10.010 (2)
c, Å	24.511 (3)	16.307 (4)	16.623 (2)	16.383 (4)
β, deg		110.30 (1)	110.33 (1)	111.20 (1)
V, Å^3	6659.5	1713.0	1743.7	1832.6
Z	8	2	2	2
T, °C	298 (1)	298 (1)	298 (1)	298 (1)
radiation (λ, Å)	0.71073	0.71073	0.71073	0.71073
ρ_{calcd}, g cm^{-3}	1.756	1.812	1.763	1.865
μ(Mo Kα), mm^{-1}	1.01	1.09	1.15	1.11
transmission	0.209–0.277	0.341–0.686	0.524–0.598	0.60–0.69
R^a	0.060	0.076	0.083	0.088
$R_w{}^b$	0.050	0.070	0.076	0.080

$^a R = \sum||F_o| - |F_c||/\sum|F_o|$. $^b R_w = \{\sum w(|F_o| - |F_c|)^2/\sum w|F_o|^2\}^{1/2}$; $w = 1/(\sigma^2(F) + 10^{-4}F^2)$.

stead of $NaPF_6$ to the reaction mixture affording **7**. Red single crystals of **8** were grown from an acetone/water (1:1) mixture containing **8** by slow evaporation in an open vessel. Intensities and lattice parameters of each of these crystals were measured at 298 (1) K on a Nicolet R 3 m/V diffractometer by using graphite monochromated Mo-Kα radiation (λ = 0.71073 Å). Crystal parameters and details of the refinement are given in Table I. Empirical absorption corrections (ψ-scans) were carried out in each case. All structures were solved by direct and Fourier methods and refined with anisotropic thermal parameters for all non-hydrogen atoms. Neutral atom scattering factors were taken from ref 23. Anomalous dispersion corrections were applied to all non-hydrogen atoms.[23] H-atom positions of methylene and methyl groups were calculated (CH_2 from geometrical considerations, CH_3 as rigid bodies) and refined with isotropic thermal parameter U = 0.08 Å^2. Both ClO_4^- anions in **6** were found to be disordered. The disorder was modeled by using a split atom model for the oxygen atoms. Two of the three ClO_4^- anions in **7** are also disordered (Cl1 and Cl3). Again a split atom model for the oxygens improved the refinement.

Results

Synthesis of Complexes. Scheme I summarizes the synthetic routes to the new asymmetric heterodinuclear complexes. Co hydrolysis of equimolar amounts of the monomeric species $L'RuCl_3\cdot H_2O$ and $LMCl_3$ (M = V, Mn, Fe, Co) in refluxing methanol containing an excess of sodium acetate yielded highly colored solutions from which upon addition of sodium hexafluorophosphate crystalline materials of the composition $[L'Ru(\mu\text{-}O)(\mu\text{-}CH_3CO_2)_2ML](PF_6)_2$ precipitated: M = Co (**1**), V (**2**), Mn (**4**), Fe (**5**). An alternative route to **4** by using $L'RuCl_3\cdot H_2O$ and $[L_2Mn_2O(CH_3CO_2)_2](PF_6)_2$ as starting materials (2:1) proved to be more efficient. Since we have not been able to generate the corresponding chromium analogue by co-hydrolysis of $L'RuCl_3\cdot H_2O$ and $LCrCl_3$ we decided to exchange the capping amine ligands. Thus, using the monomeric complexes $LRuCl_3$ and $L'CrBr_3$ as starting materials under otherwise identical reaction conditions we have isolated $[LRu(\mu\text{-}O)(\mu\text{-}CH_3CO_2)_2CrL'](PF_6)_2$ (**3**).

Reaction of **4** and **5** in aqueous solution with $Na_2[S_2O_8]$ and addition of solid $NaPF_6$ afforded crystalline materials of $[L'Ru(\mu\text{-}O)(\mu\text{-}CH_3CO_2)_2MnL](PF_6)_3$ (**6**) and $[L'Ru(\mu\text{-}O)(\mu\text{-}CH_3CO_2)_2FeL](PF_6)_3$ (**7**), respectively, which are the one-electron oxidation products of **4** and **5**.

The oxo bridge of some asymmetric heterodinuclear species is readily protonated in acidic solution with formation of μ-hydroxo species. $[L'Ru(\mu\text{-}OH)(\mu\text{-}CH_3CO_2)_2CoL](PF_6)_3$ (**8**) is produced quantitatively from an aqueous solution of **1** by addition of HPF_6 and $NaPF_6$ or from co-hydrolysis of $L'RuCl_3\cdot H_2O$, $LCoCl_3$, and sodium acetate in acidic (HPF_6) methanol solution. $[LRu(\mu\text{-}OH)(\mu\text{-}CH_3CO_2)_2CrL'](PF_6)_3$ (**9**) has been obtained similarly from **3** as has $[L'Ru(\mu\text{-}OH)(\mu\text{-}CH_3CO_2)_2FeL](PF_6)_3$ (**10**) from **5**. This protonation is reversible; the oxo bridged species **1**, **3**, and **5** formed in aqueous solutions of **8**, **9**, and **10** to which triethylamine was added, respectively.

Crystal Structures. The crystal structures of **2** and **5** have been communicated.[24] Here we report the structures of **4**, **6**, **7**, and **8**. These include examples for $[Ru^{III}OM^{III}]^{2+}$, $[Ru^{III}OM^{IV}]^{3+}$, $[Ru^{IV}OM^{III}]^{3+}$, and $[Ru^{III}(OH)M^{III}]^{3+}$ species. Table II summarizes selected bond lengths and angles of homo- and heterodinuclear complexes pertinent to the following discussion. Full details of X-ray structure determinations are available as supplementary material.

Figure 1 shows the structure and atom labeling scheme of the cation in crystals of **4**. We have chosen to show only one representative view for all X-ray structure determinations. The structures of the cations in **6**, **7**, and **8** are very similar (supplementary material); only the metrical details are of interest here (Table II). **4**, **6**, and **7** contain the heterodinuclear (μ-oxo)bis(μ-acetato)rutheniummetal structural motif whereas **8** contains a (μ-hydroxo)bis(μ-acetato)ruthenium(III)cobalt(III) entity. The ruthenium ions are capped by a tridentate 1,4,7-trimethyl-1,4,7-triazacyclononane ligand whereas the respective first-row transition

Scheme I. Synthesis of Complexes

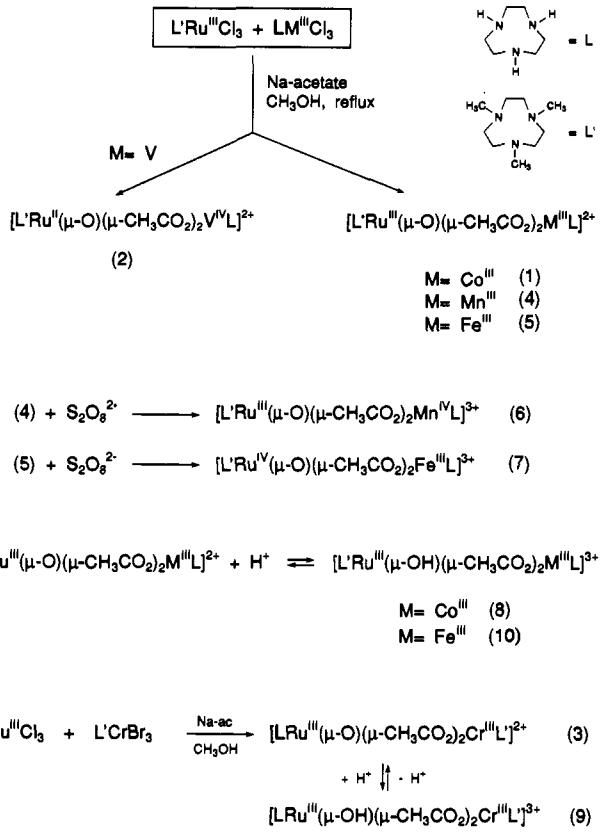

(24) Hotzelmann, R.; Wieghardt, K.; Flörke, U.; Haupt, H.-J. *Angew. Chem., Int. Ed. Engl.* **1990**, *29*, 645.

Table II. Selected Bond Distances and Angles of Hetero- and Homodinuclear Complexes

complex	M	M–N_t, Å	av M–N_c, Å	Ru–N_t, Å	av Ru–N_c, Å	M–O(H), Å	Ru–O(H), Å	M···M, Å	M–O(H)–M, deg
2	V	2.23 (1)	2.16 (1)	2.08 (1)	2.08 (1)	1.665 (8)	2.05 (1)	3.153 (3)	115.6 (5)
3	Cr	2.32 (1)	2.13 (1)	2.10 (1)	2.05 (1)	1.84 (1)	1.89 (1)	3.220 (7)	118.4 (9)
4	Mn	2.169 (7)	2.24 (1)	2.138 (7)	2.099 (7)	1.789 (5)	1.882 (5)	3.172 (1)	119.5 (3)
5	Fe	2.26 (2)	2.12 (2)	2.10 (3)	2.04 (2)	1.73 (2)	1.95 (2)	3.176 (3)	119.3 (8)
6	Mn	2.145 (7)	2.038 (8)	2.149 (9)	2.097 (7)	1.776 (5)	1.902 (7)	3.195 (2)	120.6 (4)
7	Fe	2.140 (8)	2.103 (9)	2.139 (11)	2.098 (8)	1.857 (6)	1.820 (8)	3.198 (2)	120.9 (7)
8	Co	1.925 (7)	1.934 (8)	2.095 (10)	2.112 (7)	1.932 (5)	2.032 (8)	3.431 (2)	119.8 (4)
Ru^{III}_2O[a]				2.168 (4)	2.111 (4)		1.884 (2)	3.258 (1)	119.7 (2)
$Ru^{III}_2(OH)$[b]							1.98 (2)	3.472 (2)	
V^{III}_2O[a]		2.228 (5)	2.158 (5)			1.792 (4)		3.250 (2)	130.2 (2)
Cr^{III}_2O[a]		2.165 (8)	2.128 (8)			1.850 (5)		3.219 (2)	121.0 (3)
Mn^{III}_2O[a]		2.131 (7)	2.232 (5)			1.810 (4)		3.084 (3)	120.9 (1)
Fe^{III}_2O[a]		2.268 (6)	2.198 (4)			1.800 (3)		3.120 (3)	119.7 (2)

[a] Homodinuclear complexes $[L'_2M_2(\mu\text{-}O)(\mu\text{-}CH_3CO_2)_2]^{2+}$; Ru, ref 11a; V, ref 5b; Cr, ref 6; Mn, ref 7a,b; Fe, ref 8. [b] $[L'_2Ru_2(\mu\text{-}OH)(\mu\text{-}CH_3CO_2)_2]^{3+}$, ref 11a.

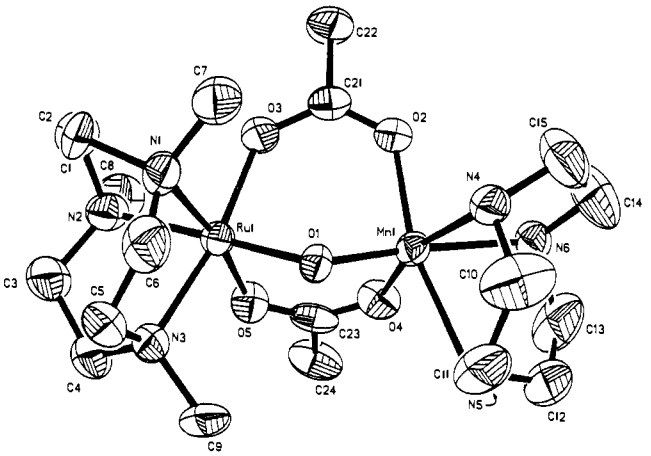

Figure 1. Structure and atom labeling scheme for the dication in crystals of **4**.

metal (Mn^{III}, Mn^{IV}, Fe^{III}, and Co^{III}) is coordinated to its unmethylated derivative 1,4,7-triazacyclononane. This general structural similarity holds irrespective of the actual charge of the asymmetric heterodinuclear cation which is +2 in **2**, **5**, and **4** and +3 in **6**, **7**, and **8**.

The dinuclear cations in the bisperchlorate salt of **5**,[24] the bisperchlorate hexafluorophosphate salt of **6**, the trisperchlorate salt of **7**, and the trishexafluorophosphate salt **8** possess a crystallographic mirror plane. The atoms Ru and metal, the oxo/hydroxo group, and one nitrogen atom of each ligand L′ and L in the trans position to the oxo/hydroxo group are located on this mirror plane. Since site symmetry *m* is not compatible with the (λλλ) or (δδδ) conformation of the three five-membered chelate rings (Ru–N–C–C–N or M–N–C–C–N) of each coordinated ligand L′ or L, a static disorder of methylene carbon atoms is observed in each case which results in apparently too short C–C single bonds and physically meaningless, large anisotropic temperature factors of these symmetry related methylene carbon atoms. In contrast, the dinuclear cations in the bishexafluorophosphate salts of **2** and **4** do not possess crystallographically imposed symmetry and, consequently, the above complication is not observed in these cases.

In the following we discuss features of each structure determination which bear relevance to the assignment of oxidation states at each metal ion. The assignment of oxidation states by X-ray crystallography in $[RuOMn]^{2+}$ (**4**) and $[RuOMn]^{3+}$ (**6**) is unambiguous. **4** contains a manganese(III) ion whereas in **6** a manganese(IV) ion is present, in addition to a ruthenium(III) ion in each structure. This is nicely borne out by the fact that the difference between the Mn–N_t bond lengths in the trans position to the oxo bridge and the average Mn–N_c distance in this cis position with respect to the oxo bridge, $\Delta[(Mn\text{–}N_t)\text{–}(Mn\text{–}N_c)]$, is –0.07 Å in **4** and +0.107 Å in **6**. Thus the oxo bridge in **4** does not exert a structural trans influence on the Mn–N bond in the trans position with respect to the oxo bridge. In **6** this trans influence is clearly observed. Interestingly, in both structures a trans influence on the Ru–N_t bond is observed: Δ = +0.039 Å in **4** and +0.059 Å in **6**. The Δ value for the symmetric homodinuclear species $[L'_2Ru_2^{III}(\mu\text{-}O)(\mu\text{-}CH_3CO_2)_2]^{2+}$ is +0.057 Å, and for the $[L'_2Mn_2^{III}(\mu\text{-}O)(\mu\text{-}CH_3CO_2)_2]^{2+}$ complex Δ = –0.10 Å. The apparent lack of a significant trans influence of the oxo bridge in all complexes containing a manganese(III) ion (d^4 high spin) has been ascribed to a tetragonal Jahn–Teller compression along the N_t–Mn–O_{oxo} axis.[7b,c] The Ru–N, Ru–$O_{acetate}$, and Ru–O_{oxo} distances in **4**, **6**, and the $[Ru^{III}\text{–}O\text{–}Ru^{III}]^{2+}$ species[11a] are within experimental error identical, thus corroborating the Ru(III) assignment. On the other hand, the Mn–N_c and Mn–$O_{acetate}$, distances in **6** are significantly shorter than those in **4** in agreement with the smaller ionic radius of Mn(IV) as compared to Mn(III).[9] A further interesting aspect is the observation that the Ru···Mn nonbonding distance in **4** increases by 0.02 Å upon oxidation to **6** despite the fact that all bonding Mn–O distances of the bridging acetate and oxo groups decrease on going from Mn(III) to Mn(IV). The Ru–O–Mn bond angle increases slightly from 119.5 (3)° in **4** to 120.6 (4)° in **6** allowing thereby a larger separation of the Ru and Mn centers in **6**. This is probably a manifestation of the increased electrostatic repulsion between the Ru(III) and Mn(IV) ions in **6** as compared to Ru(III)Mn(III) in **4**.

As has been communicated previously,[24] $[RuOV]^{2+}$ (**2**) contains a very asymmetric oxo bridge; the V–O_b distance is extremely short at 1.665 (8) Å, indicating considerable double bond character, and the Ru–O_b at 2.05 (1) Å is quite long as compared to all other μ-oxo ruthenium(III) complexes. Note that the V–O_{oxo} distance in $[L'_2V_2^{III}(\mu\text{-}O)(\mu\text{-}CH_3CO_2)_2]^{2+}$ is 1.792 (4) Å.[5b] Interestingly, the difference $\Delta[(Ru\text{–}N_t)\text{–}(Ru\text{–}N_c)]$ in **2** is zero, indicating the absence of a trans influence; on the other hand, $\Delta[(V\text{–}N_t)\text{–}(V\text{–}N_c)]$ is +0.07 Å. These structural features are in agreement with the formulation of **2** as the $[Ru^{II}\text{—}O{=}V^{IV}]^{2+}$ complex.

The structure of $[RuOFe]^{2+}$ (**5**) indicates the presence of an iron(III) and a ruthenium(III) ion. The metrical details of the coordination sphere around the iron(III) in **5** are very similar to those of its homodinuclear counterpart $[L_2Fe_2^{III}(\mu\text{-}O)(\mu\text{-}CH_3CO_2)_2]^{2+}$—with the exception of a somewhat shorter Fe–O_{oxo} distance in **5**.[8b,c] The Δ values at the iron and ruthenium center are +0.14 and +0.06 Å, respectively, which agree nicely with those found for the homodinuclear species $[Ru_2^{III}O]^{2+}$ and $[Fe_2^{III}O]^{2+}$ of +0.057 Å. The larger Δ_{Fe} value for **5** as compared to $[Fe_2^{III}O]^{2+}$ is a consequence of the shorter Fe–O_{oxo} distance in **5**.

One-electron oxidation of **5** to $[RuOFe]^{3+}$ (**7**) brings about the following major structural differences: (i) the Ru–O_{oxo} distance decreases by 0.13 Å, whereas the Fe–O_{oxo} bond length increases by 0.127 Å; (ii) as a consequence of this and Δ_{Fe} value of **7** of 0.037 Å is smaller than that in **5**; and the Δ_{Ru} value of **7** of 0.040 Å is marginally smaller than that in **5**. The fact that the bridging oxo atom moves closer to the ruthenium center and away from the iron center is taken as evidence that the Ru ion is oxidized

Table III. Electrochemical Data of Complexes[a]

complex	$E_{1/2}$,[b] V vs NHE	E_{red},[c] V vs NHE	ref
1	+0.51 r	−0.85 irr	this work
2	+0.46 r	−1.44 qr	this work
3	+0.48 qr		this work
4	+0.60 r	−0.92 irr	this work
5	+0.59 r	−0.91 irr	this work
6	same behavior as **4**		this work
7	same behavior as **5**		this work
8	+0.04 qr	−0.81 irr	this work
9	±0.00 r		this work
10	+0.19 r		this work
Ru^{III}_2O	+0.59 r	−1.15 irr	11a
$L'_2Mn^{III}_2O$	+0.985 r	−0.10 irr	7a,d
$L_2Mn^{III}_2O$	+0.68 r		7a,d
V^{III}_2O	+0.38 r	−1.47 r	5a

[a] Cyclic voltammetric measurements in CH_3CN solution at 20 °C (Pt-button electrode; 0.10 M $[TBA]PF_6$ supporting electrolyte; [complex] ~ 10^{-3} M; ferrocenium/ferrocene couple internal standard); r = reversible; irr = irreversible; qr = quasireversible. [b] Formal redox potential $E_{1/2} = (E_{p,a} + E_{p,c})/2$. [c] Peak potential of reduction peak.

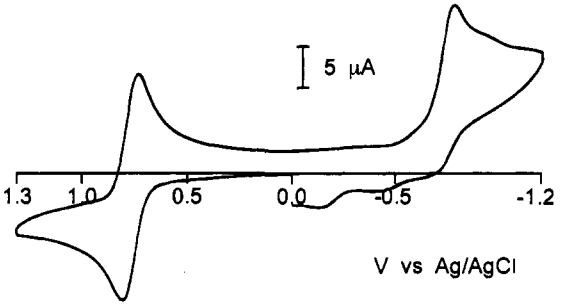

Figure 2. Cyclic voltammogram of **4** in acetonitrile at 20 °C ([**4**] ≈ 10^{-3} M, 0.10 M $[TBA]PF_6$ supporting electrolyte, Pt-button working electrode, scan rate 200 mV s^{-1}).

on going from **6** to **7**. The nonbonding Ru···Fe distance is longer by 0.022 Å in **7** than in **5** which again indicates the increased electrostatic repulsion between the metal ions.

8 is the only μ-hydroxo complex investigated in the present series. It is well established that protonation of an oxo bridge leads to significantly elongated M–O_b bond distances in the resulting hydroxo bridged compound. Thus the Ru–$O_{hydroxo}$ bond in **8** is longer by ~0.10 Å than the corresponding Ru–O_{oxo} distance.[11a] Similar effects have been demonstrated for the dinuclear couple $[(HBpz_3)Fe(\mu\text{-}O)(\mu\text{-}CH_3CO_2)_2Fe(HBpz_3)]$ and $[(HBpz_3)Fe(\mu\text{-}OH)(\mu\text{-}CH_3CO_2)_2Fe(HBpz_3)]^+$ and other complexes of this type.[19,25] Common for μ-hydroxo species is also the lack of a significant structural trans influence of the μ-OH bridge on the M–N_t bond in the trans position with respect to the OH group. This is also observed for **8**. The Co–N and Co–O distances are typical for cobalt(III); they are shorter by ~0.20 Å than the corresponding Co^{II}–L distances.[26] Thus **8** is a $[Ru^{III}(OH)Co^{III}]^{3+}$ species.

Finally, we note that the preliminary structural data on $[RuOCr]^{2+}$ (**3**)[27] show that a $[Ru^{III}OCr^{III}]^{2+}$ species is formed. Considering the usual redox stability of octahedral chromium(III) complexes this result is not surprising.

Table IV. Electronic Spectra of Complexes[a]

complex	λ, nm (ε, L mol^{-1} cm^{-1})
1	600 (1.0×10^3), 458 (1.0×10^4)
2	700 sh (1.3×10^3), 556 (1.8×10^3), 360 sh (1.65×10^3), 249 (6.3×10^3)
3	780 sh (660), 741 (1.3×10^3), 620 (130), 590 sh (420), 524 (840), 380 (5.0×10^3)
4	721 (2.4×10^3), 516 (1.4×10^3), 394 (8.4×10^3)
5	1260 (180), 534 (5.1×10^3), 405 (5.2×10^3), 295 (3.8×10^3)
6	830 (1.35×10^3), 648 (2.1×10^3), 454 (5.2×10^3), 350 sh (5.3×10^3), 270 sh (8.6×10^3)
7	941 (300), 529 (2.9×10^3), 380 (5.3×10^3), 320 (6.5×10^3), 300 (6.6×10^3)
8	520 (310), 401 (2.35×10^3)
9	699 (36), 690 (32), 670 (31), 650 (22), 630 sh (18), 480 (170), 350 sh (1.1×10^3)
10	520 sh (530), 480 (580), 440 sh (600), 330 sh (2.4×10^3)

[a] Measured in CH_3CN solution at 20 °C in the range 240–1500 nm.

Electrochemistry. Table III gives electrochemical data of certain complexes. Cyclic voltammograms (cv) on acetonitrile solutions containing 0.10 M tetra-*n*-butylammonium hexafluorophosphate as supporting electrolyte and ≈10^{-3} M complex have been recorded in the range +1.60 to −1.60 V vs Ag/AgCl with scan rates of 20–200 mV/s. Figure 2 shows a representative cv of **4**.

It is striking that all oxo bridged heterodinuclear complexes, **1**–**7**, show a reversible (or quasireversible; **3**) one-electron oxidation wave in a rather narrow potential range of 0.46–0.60 V vs NHE irrespective of the nature of the first-row transition metal, eq 1a. The peak potential difference is 70 mV for all complexes, and the ratio I_{pc}/I_{pa} is 1.0 ± 0.1 at scan rates of 20–200 mV/s. The μ-hydroxo species **8**, **9**, and **10** show a one-electron *reduction* wave (eq 1b). The oxo bridged complexes are all irreversibly reduced

$$[RuOM]^{2+} \rightleftarrows [RuOM]^{3+} + e^- \quad (1a)$$

$$[RuOHM]^{3+} + e^- \rightleftarrows [RuOHM]^{2+} \quad (1b)$$

by one electron at quite negative potentials. We will not discuss this step in the following. It is noted that complex **6** shows the same cv as **4** and **7** the same cv as **5**.

We have included in Table III electrochemical data for the homodinuclear complexes $[L'_2Ru_2^{III}(\mu\text{-}O)(\mu\text{-}CH_3CO_2)_2]^{2+}$, $[L'_2Mn_2^{III}(\mu\text{-}O)(\mu\text{-}CH_3CO_2)_2]^{2+}$, $[L_2Mn_2^{III}(\mu\text{-}O)(\mu\text{-}CH_3CO_2)_2]^{2+}$, and $[L'_2V_2(\mu\text{-}O)(\mu\text{-}CH_3CO_2)_2]^{2+}$, all of which display a reversible one-electron oxidation wave, eq 2. The $E_{1/2}$ values for this process

$$[M_2^{III}O]^{2+} \rightleftarrows [M^{III}OM^{IV}]^{3+} + e^- \quad (2)$$

for the homodinuclear ruthenium, vanadium, and manganese complexes are quite similar to those found for the heterodinuclear species. One-electron oxidation of the dinuclear species produces mixed valent compounds with localized valences in the manganese and, probably, vanadium cases. $[RuORu]^{3+}$, in contrast, is probably a complex with delocalized valences, $[Ru^{3.5}ORu^{3.5}]^{3+}$.[11a] This electronic difference is not reflected in the electrochemical behavior of the complexes. This raises then the following question: Which of the metal ions is oxidized in the heterodinuclear complexes—the first-row transition metal or the ruthenium ion?

In some instances it is possible to assign oxidation states in the electrochemically generated oxidized forms $[RuOM]^{3+}$ on the basis of a usually inaccessible oxidation state of the first-row transition metal. Thus for **1** we consider it highly unlikely that a $[Ru^{III}O\text{-}Co^{IV}]^{3+}$ species is formed which would contain a very unusual octahedral cobalt(IV) ion. $[RuOCo]^{3+}$ is probably $[Ru^{IV}OCo^{III}]^{3+}$. We have not yet been able to isolate and characterize this species. Following the same reasoning the oxidized forms of **3** and **5** should be described as $[Ru^{IV}OCr^{III}]^{3+}$ and $[Ru^{IV}OFe^{III}]^{3+}$, respectively. The latter species has been isolated as crystalline solid **7**, and its electronic and structural properties corroborate the above assignment of oxidation states (see below). On the other hand, oxidation of **4** yields **6** containing undoubtedly a manganese(IV)

(25) Armstrong, W. H.; Lippard, S. J. *J. Am. Chem. Soc.* **1984**, *106*, 4632.
(26) Chaudhuri, P.; Querbach, J.; Wieghardt, K.; Nuber, B.; Weiss, J. *J. Chem. Soc., Dalton Trans.* **1990**, 271.
(27) The structure of $[LRu(\mu\text{-}O)(\mu\text{-}CH_3CO_2)_2CrL'](ClO_4)_2$ (**3**) has been determined by X-ray crystallography. Crystal data: orthorhombic space group *Pnma*, a = 9.979 (2) Å, b = 14.660 (5) Å, c = 22.717 (4) Å; V = 3323.5 Å^3, Z = 4. The crystals were of low quality and the ClO_4^- ions were found to be severely disordered which could not be satisfactorily modeled. The present R value is 0.14. Despite these presently unresolvable problems the atom connectivity of the dication in **3** has been unambiguously established. Preliminary bond distances (Å) are the following: Ru–O_{oxo} 1.87 (1); Cr–O_{oxo} 1.80 (2); Ru···Cr 3.22 (1).
(28) Wieghardt, K.; Bossek, U.; Chaudhuri, P.; Herrmann, W.; Menke, B. C.; Weiss, J. *Inorg. Chem.* **1982**, *21*, 4308.

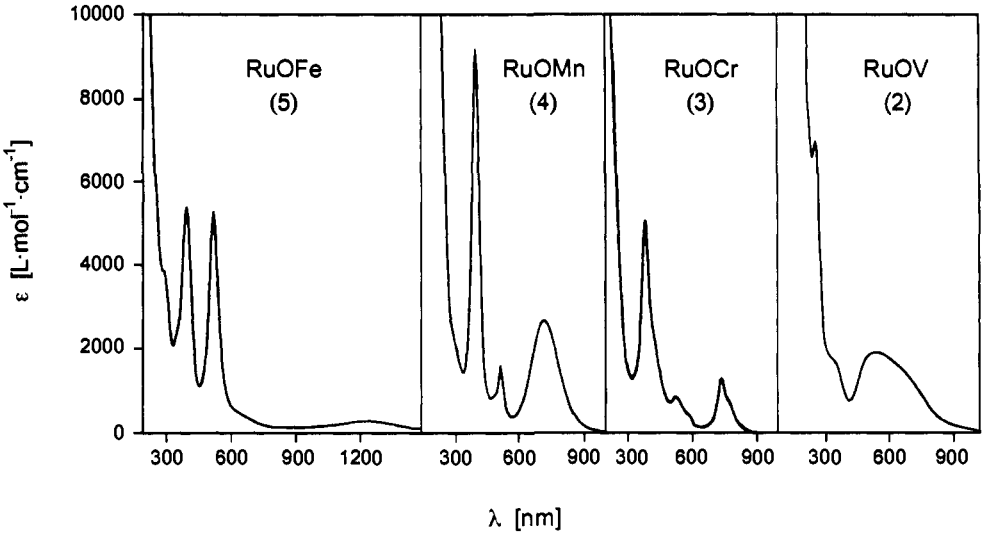

Figure 3. UV–vis spectra of **2**, **3**, **4**, and **5** in acetonitrile at ambient temperature.

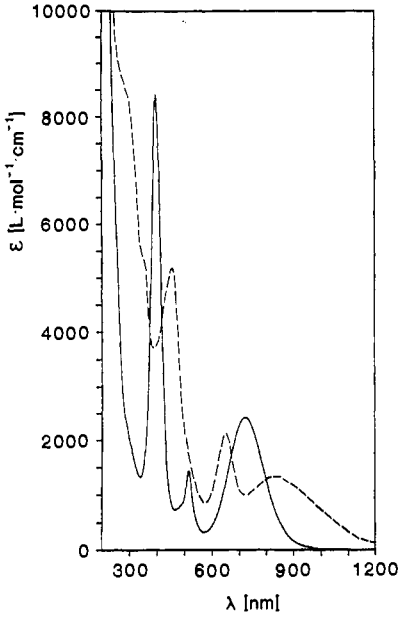

Figure 4. UV–vis spectra of **4** (—) and **6** (---) in acetonitrile at ambient temperature.

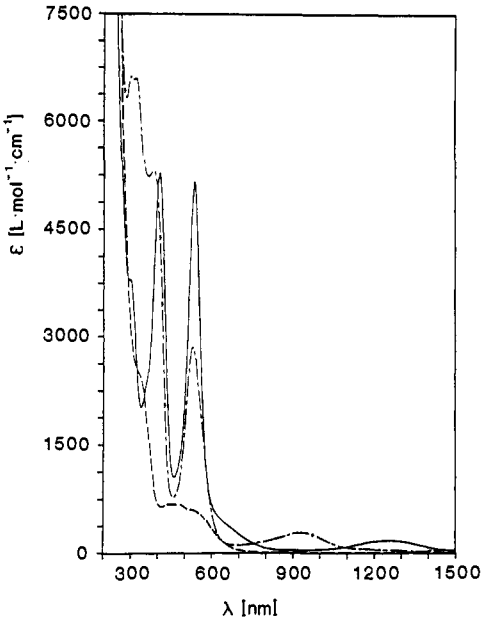

Figure 5. UV–vis spectra of **5** (—), **7** (-·-), and **10** (---) in acetonitrile at ambient temperature.

ion. In this case the first-row transition metal and not Ru(III) is oxidized.

The hydroxo bridged complexes **8**, **9**, and **10** display a reversible one-electron reduction in the potential range of 0.00–0.20 V vs NHE. Since octahedral chromium(III) complexes in a N_3O_3 ligand environment are generally reduced at much more negative potentials[29] we propose that a $[Ru^{II}(OH)Cr^{III}]^{2+}$ species is electrochemically generated from **9**. For **8** both formulations $[Ru^{II}(OH)Co^{III}]^{2+}$ and $[Ru^{III}(OH)Co^{II}]^{2+}$ are conceivable. The same situation is encountered for reduced **10**. Without isolation and characterization of these reduced forms the assignment of oxidation states remains ambiguous. Attempts to isolate crystalline materials from electrochemically reduced **8**, **9**, and **10** were unsuccessful.

Electronic Spectra. UV–vis absorption spectra of acetonitrile solutions of the complexes were recorded in the range 250–1200 nm at ambient temperature. Table IV gives absorption maxima and molar absorption coefficients.

All $[RuOM]^{2+}$ oxo bridged complexes **1–7** are deeply colored; their electronic absorption spectra display a number of absorption maxima in the visible with unusually large molar absorption coefficients ($>10^3$ M^{-1} cm^{-1}) considering the simple N_3O_3 ligand environment at both metal ions. The local C_{2v} symmetry at each metal ion certainly relaxes the Laporte selection rule for d–d transitions, but this alone cannot account for the observed intensity of the most intense absorption maxima. Figure 3 shows the spectra of **2**, **3**, **4**, and **5**. Even a superficial comparison immediately indicates that the spectrum of **2** differs in character from those of the other complexes. The spectra of **5**, **4**, **3**, and **1** display at least one very intense absorption in the range 380–460 nm with a molar absorption coefficient between 10^3 and 10^4 L mol^{-1} cm^{-1} which is also observed for the oxidized $[RuOM]^{3+}$ species **6** and **7** but is lacking in the spectrum of **2**. This band appears to be typical for $[Ru^{III/IV}OM]^{2+/3+}$ complexes and has oxo-to-$Ru^{III/IV}$ charge-transfer character. In the spectra of the homodinuclear species $[RuORu]^{2+}$ and $[RuORu]^{3+}$ this absorption is observed at 542 (6.1×10^3 L mol^{-1} cm^{-1}) and 478 nm (5.7×10^3 L mol^{-1} cm^{-1}), respectively.[11a]

Figures 4 and 5 show the spectral changes which occur upon one-electron oxidation of **4** to **6** and **5** to **7**, respectively. The first process involves oxidation of the manganese ion ($Mn^{III} \rightarrow Mn^{IV}$) whereas in the latter the ruthenium ion is oxidized ($Ru^{III} \rightarrow Ru^{IV}$) (see below).

(29) Figgis, B. N.; Lewis, J.; Mabbs, F. E.; Webb, G. A. *J. Chem. Soc. (A)* **1966**, 422.

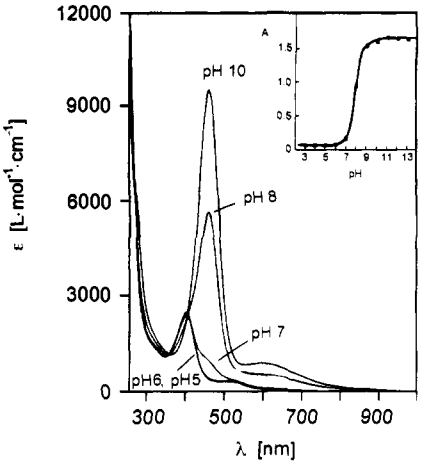

Figure 6. UV–vis spectra of **1** and its protonated form **8** in H_2O as a function of pH. The inset shows the change of absorption at 458 nm as a function of pH.

Table V. Magnetic Properties of Complexes[a]

complex	μ_{eff}/μ_B 295 K	μ_{eff}/μ_B 10 K	S_t (ground state)
$[CoORu]^{2+}$ (**1**)	2.16	1.92	$^1/_2$
$[VORu]^{2+}$ (**2**)	1.63	1.63	$^1/_2$
$[CrORu]^{2+}$ (**3**)	2.82	2.66	1
$[MnORu]^{2+}$ (**4**)	3.87	3.92	$^3/_2$
$[FeORu]^{2+}$ (**5**)	4.79	4.15	2
$[MnORu]^{3+}$ (**6**)	3.23	2.81	1
$[FeORu]^{3+}$ (**7**)	4.01	3.75	$^3/_2$
$[Co(OH)Ru]^{3+}$ (**8**)	2.54	2.28	$^1/_2$
$[Cr(OH)Ru]^{3+}$ (**9**)	4.25	2.77	1
$[Fe(OH)Ru]^{3+}$ (**10**)	6.30	6.00	2

[a] Full details are available in the supplementary material.

The spectrum of **3** is remarkable in the sense that three fairly intense spin-forbidden d–d transitions of pseudooctahedral chromium(III) are observed in the range 800–600 nm ($^4A_2 \rightarrow {}^2E$ transition). This has also been observed for the homodinuclear complex $[L'_2Cr_2(\mu\text{-}O)(\mu\text{-}CH_3CO_2)_2]^{2+}$.[6]

Protonation of the oxo bridges in **1**, **3**, and **5** affords the μ-hydroxo species **8**, **9**, and **10**. This relatively small chemical perturbation has a dramatic effect on the electronic spectra. The very intense absorption maxima in the visible described above vanish completely. Figure 6 shows this effect for the **1** → **8** transformation. From the pH dependence of the dramatic color change (inset, Figure 6) a dissociation constant for the hydroxo group was determined spectrophotometrically at 20 °C, eq 3. A

$$[Ru(OH)M]^{3+} \rightleftarrows [RuOM]^{2+} + H^+ \qquad (3)$$

pK_a value of 8.0 for **8** has been determined whereas for **9** and **10** values of 7.5 and 4.0 have been found. The homodinuclear species $[Ru_2^{III}(OH)]^{3+}$ has a pK_a value of 1.9,[1a] and the value for its vanadium(III) analogue $[V_2^{III}OH]^{3+}$ is 0.9.[5d] Thus the basicity of the oxo bridges varies over a range of eight orders of magnitude. This effect may reflect the π-donor capability of the oxo group. In the $[RuOM]^{2+}$ series **1** contains a cobalt(III) ion with a filled t_{2g} shell (d^6 low spin) which cannot form π-donor interactions with the O^{2-} ligand. Thus **1** has the most basic oxo bridge. Removal of electrons from the t_{2g} orbitals of the first-row transition-metal ion increases the π-donor capability and the oxo bridge becomes less basic.

Magnetochemistry. Temperature-dependent magnetic susceptibilities of complexes **1–10** have been measured in the range 4–295 K. Magnetic moments as a function of temperature of the μ-oxo complexes **1–7** are shown in Figure 7; Figure 8 displays the data of the μ-hydroxo complexes **8–10**. Table V summarizes effective magnetic moments and gives the electronic ground states of the dinuclear cations.

Mononuclear octahedral Ru(III) complexes have a low-spin t^5_{2g} electronic configuration with one unpaired electron ($S = {}^1/_2$).

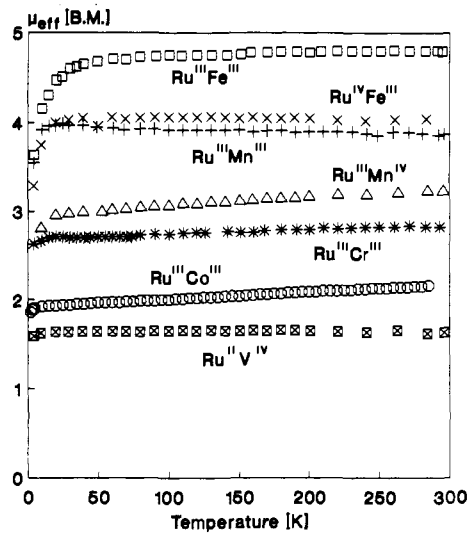

Figure 7. Temperature dependence of magnetic moments of μ-oxo complexes $[RuOM]^{n+}$: □, **5**; ×, **7**; +, **4**; △, **6**; ✱, **3**; ○, **1**; □, **2**.

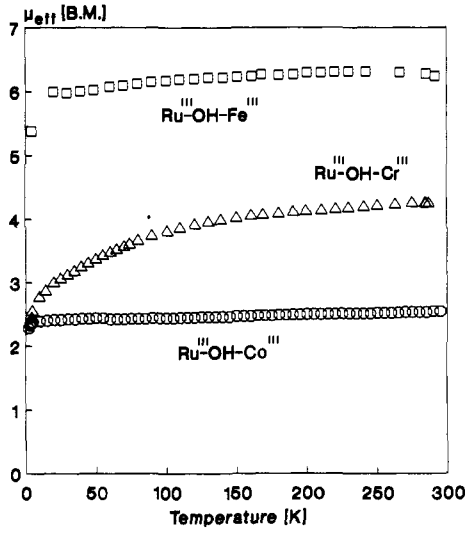

Figure 8. Temperature dependence of magnetic moments of μ-hydroxo complexes $[Ru(OH)M]^{3+}$: □, **10**; △, **9**; ○, **8**.

Magnetic moments are usually somewhat temperature dependent;[29] they can vary between 1.7 and 2.5 μ_B in the range 5–300 K. Ru(II) complexes, on the other hand, are diamagnetic (t^6_{2g}; $S = 0$). Complexes **1** and **8** contain a diamagnetic low-spin cobalt(III) ion and a pseudooctahedral ruthenium(III) ion; both complexes have one unpaired electron per dinuclear unit which is located at the ruthenium ion and, consequently, the observed temperature dependence and the increased numerical values of the magnetic moments at room temperature—as compared to the spin-only value of 1.73 μ_B—are quite typical for octahedral ruthenium(III) complexes.

The $[RuOV]^{2+}$ complex **2** shows a temperature-independent magnetic moment of 1.635 μ_B (9.1–296 K). This value is a little smaller than the spin-only value for an $S = {}^1/_2$ species. As has been shown by X-ray crystallography and its electronic spectrum, **2** contains a diamagnetic low-spin ruthenium(II) and a pseudooctahedral vanadyl (d^1) moiety. The susceptibility data corroborate this assignment nicely.[30] Vanadyl complexes typically have magnetic moments close to the spin-only value of 1.73 μ_B.

Despite the fact that all other oxo bridged $[RuOM]^{2+/3+}$ complexes (**3**, **4**, **5**, **6**, and **7**) contain *two* paramagnetic ions (Ru(III) or Ru(IV) and M(III) or M(IV)), we observe rather simple magnetochemical behavior. The magnetic moments are only slightly temperature dependent, contrasting in this respect

(30) Figgis, B. N.; Lewis, J. *Progr. Inorg. Chem.* **1964**, *6*, 37.

the heterodinuclear first-row transition-metal containing analogues.[9] By using the simple spin-only expression $\mu = [n(n+2)]^{1/2}\mu_B$ where n is the number of unpaired electrons per dinuclear unit, we arrive at the following conclusion: $[RuOCr]^{2+}$ (**3**) has two unpaired electrons, $[RuOMn]^{2+}$ (**4**) has three, $[RuOFe]^{2+}$ (**5**) has four, $[RuOMn]^{3+}$ (**6**) has two, and $[RuOFe]^{3+}$ (**7**) has three.

These magnetic data can be interpreted in either of the following two models. Very strong intramolecular antiferromagnetic spin exchange coupling between a Ru(III) (d^5 l.s.) and a trivalent first-row transition metal (Cr(III) d^3, Mn(III) d^4 h.s.; Fe(III) d^5 h.s.) occurs in complexes **3**, **4**, and **5** which yields $S = 1$, $^3/_2$, and 2 ground states, respectively. In the isotropic Heisenberg, Dirac, van Vleck model using the simple Hamiltonian $H = -2JS_1S_2$, where S_1 and S_2 represent the total spin at metal 1 and metal 2 and J is the spin exchange coupling constant in cm^{-1}, the numerical value of $|J|$ must be greater than $\sim 200\ cm^{-1}$ because the observed magnetic moments are temperature independent up to 295 K. For **6** where a Ru(III) and a Mn(IV) are present an $S = 1$ ground state results by using this antiferromagnetic coupling model. For **7** the situation is slightly more complex since the electronic configuration of a presumed octahedral Fe(IV)–O_{oxo} species is not known. It could have four or two unpaired electrons, and antiferromagnetic coupling to a ruthenium(III) would then yield either an $S = ^1/_2$ or $^3/_2$ ground state. Since the latter is observed, the ferryl site would have to be high spin which is rather unlikely. If, on the other hand, one-electron oxidation of **5** occurs at the ruthenium ion a Ru(IV)–O–Fe(III) moiety would be present in **7**. Hatfield et al.[31] have recently shown for a mononuclear octahedral ruthenium(IV) complex containing a terminal oxo ligand that it has an $S = 1$ ground state (2 unpaired electrons). If this ruthenium spin would be antiferromagnetically coupled to a high-spin ferric ion again an $S = ^3/_2$ ground state would be obtained. Magnetic susceptibility data alone cannot discern between the two possibilities for **7**.

The second model which envisages an intramolecular one-electron reduction of ruthenium(III) yielding a diamagnetic low-spin Ru(II) with concomitant one-electron oxidation of the first-row transition metal would also be in agreement with the magnetic susceptibility data. Complex **2** could then be formulated as $[Ru^{II}OV^{IV}]^{2+}$, **3** as $[Ru^{II}OCr^{IV}]^{2+}$, **4** as $[Ru^{II}OMn^{IV}]^{2+}$, and **5** as $[Ru^{II}OFe^{IV}]^{2+}$ where V(IV) would provide one unpaired electron ($S = ^1/_2$), Cr(IV) two electrons ($S = 1$), Mn(IV) three electrons ($S = ^3/_2$), and Fe(IV) four electrons ($S = 2$). By using this model **6** could be formulated as $[Ru^{II}OMn^{V}]^{3+}$ with two unpaired electrons ($S = 1$) and, finally, **7** would be a $[Ru^{II}OFe^{V}]^{3+}$ species with three unpaired electrons ($S = ^3/_2$).

Some of these formulations as those for **3**, **5**, **6**, and **7** are of course counterintuitive to our general chemical experience which tells us that octahedral ruthenium(II) complexes with σ-donor ligands are, in general, quite potent one-electron reducing agents and Cr(IV), Fe(IV), Mn(V) in the same ligand environment are surely strong oxidants. On the other hand, the presence of the oxo bridge with its π-donor capacity may stabilize thermodynamically M(IV)=O—Ru^{II} or even M(V)=O—Ru^{II} entities. This is certainly the case in **2** which contains the Ru(II)—O= V(IV) group.

The magnetism of the two hydroxo bridged complexes **9** and **10** is interesting in comparison with their oxo bridged analogs **3** and **5**. As is shown in Figure 8 the magnetic moments of both **9** and **10** are temperature dependent. For **9** μ decreases from 4.25 μ_B at 285 K to 2.6 μ_B at 5.5 K whereas for **10** 6.24 μ_B at 293 K and 5.38 μ_B at 4.2 K are observed. Since the oxidation states in **9** are $[Ru^{III}OHCr^{III}]^{3+}$, it is possible to calculate spin-only magnetic moments assuming (i) an uncoupled and (ii) a fully coupled system. If the spins in **9** and **10** are uncoupled the effective magnetic moments arising from $Ru^{III}Cr^{III}$ and $Ru^{III}Fe^{III}$ may be calculated by using the expression $\mu = (\mu_1^2 + \mu_2^2)^{1/2}$ where μ_1 and μ_2 represent the spin-only magnetic moments for Ru(III) (1.73 μ_B), Cr(III) (3.87 μ_B), and Fe(III) (5.90 μ_B). For **9** μ is then calculated as 4.24 μ_B and for **10** $\mu = 6.15\ \mu_B$. Both values are close to the observed effective magnetic moments at room temperature. Complete coupling at very low temperatures would yield 2.83 μ_B for **9** ($S = 1$) and 4.9 μ_B for **10** ($S = 2$) which again are close to the observed values. Thus, we conclude that **9** and **10** are weakly antiferromagnetically coupled.

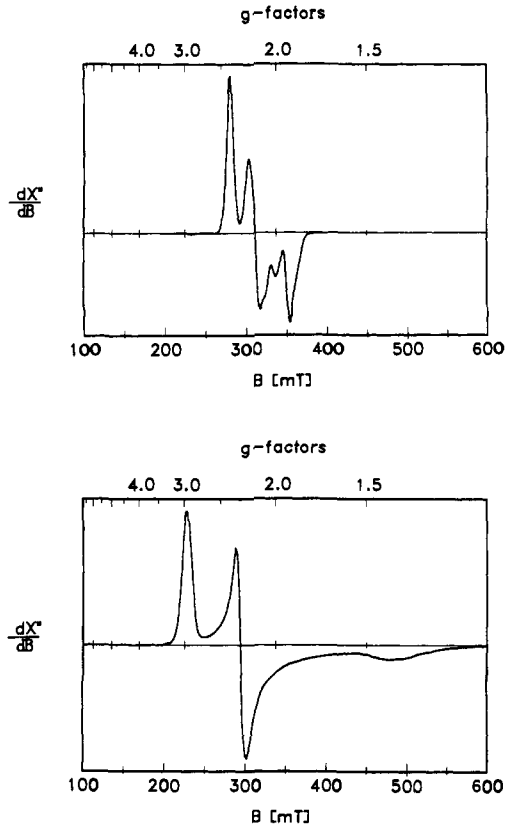

Figure 9. Top: X-band EPR spectrum of a solid sample of **1** at 10 K (microwave frequency 9.4382 GHz; power = 20.0 μW). Bottom: EPR spectrum of an acetonitrile glass of **8** at 3.4 K (microwave frequency = 9.4339 GHz; power = 20.0 μW).

Attempts to fit the magnetic susceptibility data to the isotropic Heisenberg, Dirac, van Vleck model ($H = -2JS_1 \cdot S_2$, where $S_1 = ^1/_2$ (Ru^{III}) and $S_2 = ^3/_2$ (Cr^{III}) or $^5/_2$ (Fe^{III}); $g = 2.0$ (fixed)) were successful although it is noted that this model may not be the best to calculate χ_M for complexes containing second-row transition metals.

By using eq 4 for complex **9** and eq 5 for complex **10**[32] we

$$\chi_M = \frac{Ng^2\mu_B^2}{kT}\frac{2 + 10e^{4x}}{3 + 5e^{4x}} \tag{4}$$

$$\chi_M = \frac{Ng^2\mu_B^2}{kT}\frac{10 + 28e^{6x}}{5 + 7e^{6x}}, \qquad x = J/kT \tag{5}$$

obtained reasonable fits with J values of $-15\ cm^{-1}$ for **9** and $-1\ cm^{-1}$ for **10**. The former is quite similar to values reported for (μ-hydroxo)bis(μ-carboxylato)dichromium(III) complexes.[19,33,34]

EPR Spectroscopy. X-band spectra of solid samples of complexes have been measured at low temperatures (3.4–10 K) in order to establish the electronic ground state of oxo and hydroxo bridged heterodinuclear complexes. Figure 9 shows the spectra of the simplest cases $[Ru^{III}OCo^{III}]^{2+}$ (**1**) and $[Ru^{III}OHCo^{III}]^{3+}$ (**8**). The spectrum of **1** displays a rhombic signal of an $S = ^1/_2$ ground state with $g_1 = 2.41$, $g_2 = 2.18$, and $g_3 = 1.9$. The relatively

(31) Dobson, J. C.; Helms, J. H.; Doppelt, P.; Sullivan, B. P.; Hatfield, W. E.; Meyer, T. J. *Inorg. Chem.* **1989**, *28*, 2200.
(32) O'Connor, C. J. *Progr. Inorg. Chem.* **1982**, *29*, 203.
(33) Reber, C.; Güdel, H. U.; Buijs, M.; Wieghardt, K.; Chaudhuri, P. *Inorg. Chem.* **1988**, *27*, 2115.
(34) Turowski, P. N.; Bino, A.; Lippard, S. J. *Angew. Chem., Int. Ed. Engl.* **1990**, *29*, 811.

small line width and the lack of hyperfine splitting by the ^{59}Co nucleus ($I = {}^7/_2$) is a clear indication that **1** is a genuine $[Ru^{III}OCo^{III}]^{2+}$ species with localized Ru(III), Co(III) oxidation states. The X-band spectrum of an acetonitrile glass of **8** displays also a rhombic signal with $g_1 = 2.95$, $g_2 = 2.3$, and $g_3 = 1.39$; again no line broadening or hyperfine splitting arising from ^{59}Co is observed. Both spectra are fully in accord with an octahedral Ru(III) complex of low symmetry with an $S = {}^1/_2$ ground state.[35]

Correlations of the measured g values with structural properties can be achieved by a ligand-field description of the $d(t_{2g})^5$ configuration of Ru(III).[35a] Due to a strong octahedral ligand field the t_{2g} and e_g levels are well separated and a $t_{2g}{}^5$ electron configuration prevails. The t_{2g} orbitals are also split by tetragonal components of the ligand field. The spin orbital states of such a system are just those of a (positive) hole in the t_{2g} shell. Spin-orbit coupling mixes orbital functions and yields three states (Kramers doublets), which are separated by tetragonal splittings Δ and V. We used the formalism of Taylor[36] to find the nature of the ground-state doublet and to parametrize the ligand-field splittings. The model yields analytical equations. However, it does not include orbital reduction factors to account for covalency effects. Instead, the equations are based on non-normalized wave functions which can tolerate covalent bonds to a limited extent. The advantage of the procedure is its insensitivity to propagated errors of g values, which are a severe problem in sophisticated formalisms.[35a,36] At least the simple parametrization can serve for comparison of data from complexes with similar structures. In systems without 3- or 4-fold symmetry axes, such as **1** and **8**, there are 48 possibilities to assign the measured g values g_1, g_2, g_3 with different signs to Cartesian coordinates. For both complexes we probed these combinations and calculated the corresponding spin-orbital wave functions and their energies. Using the selection criteria[36] that the wave functions should be close to normalization, that $g_z + g_y - g_x$ should be positive, and that the rhombicity factor V/Δ should be less than ${}^2/_3$, we find two quasiequivalent solutions for each complex. The ground spin doublet in any case is a nearly pure d_{xy} state, which is separated by $\Delta = 6.8\lambda$ (**1**) and 2.6λ (**8**) from the excited "d_{xz}" and "d_{yz}" levels. The rhombic splitting V of the excited states is 4.3λ in **1** and 1.8λ in **8**. The energies, given in units of the spin-orbit coupling constant λ, can be converted into absolute units by taking approximately $\lambda = 884$ cm^{-1} from $RuCl_3$.[35a] The solutions for each complex are only ambiguous in the sequence of the excited states, and in the resulting assignment of g tensor components: $g = (-2.41, 2.18, -1.9)$ or $(-2.18, 2.41, -1.9)$ for **1** and $g = (-2.95, 2.3, -1.39)$ or $(-2.3, 2.95, -1.39)$ for **8**. In any case, the lowest value is always the z component. The coefficients of the calculated spin-orbital wave functions proved to deviate from normalization by less than 0.5%. Such small departures correspond to small orbital reduction, which we can take as a justification of the procedure in retrospect. We note that small orbital reduction effects are not unusual for Ru(III) complexes due to compensating contributions to the orbital reduction factors.[35a]

The arrangement of orbital states indicates that the z axis of the ligand field in both complexes is directed along the strong Ru–O bond or Ru–OH bond, respectively. In this orientation the Ru d_{xz} and d_{yz} orbitals form π-bonds with oxygen $p_{x,y}$ orbitals and therefore rise in energy above d_{xy}. The significant reduction of tetragonal splitting in **8** with respect to that in **1** reflects the reduction of π overlap upon protonation of the μ-oxo ligand.

The susceptibility data of **2** also indicate an $S = {}^1/_2$ ground state. The EPR spectrum of the solid bis(tetraphenylborate) salt of **2** is shown in Figure 10 (bottom). The spectrum is centered at $g \approx 2$ and exhibits a prominent hyperfine splitting due to interaction with the ^{51}V nucleus ($I = {}^7/_2$). A simulation with slightly rhombic g values (1.947, 1.955, 2.01) and hyperfine

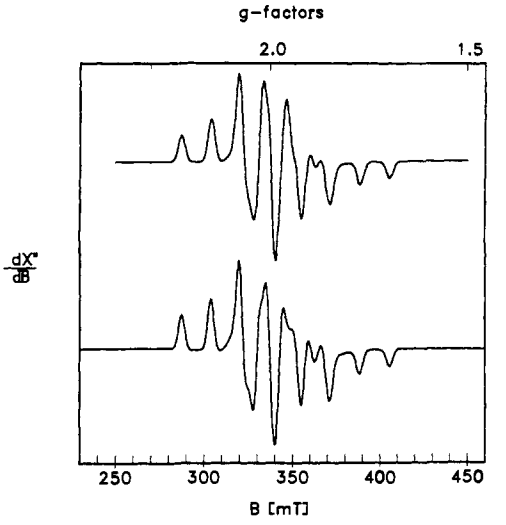

Figure 10. Bottom: Experimental X-band EPR spectrum of a solid sample of $[L'Ru(\mu\text{-}O)(\mu\text{-}CH_3CO_2)_2VL](BPh_4)_2$ (**2**) recorded at 10 K (microwave frequency = 9.4378 GHz, power = 2 μW). Top: Simulation using $g_i = (1.947, 1.955, 2.01)$, $A_i = (153.6, 60.5, 39.4) \times 10^{-4}$ cm^{-1} ($I = {}^7/_2$), $i = 1, 2, 3$; isotropic line width 2.3 mT.

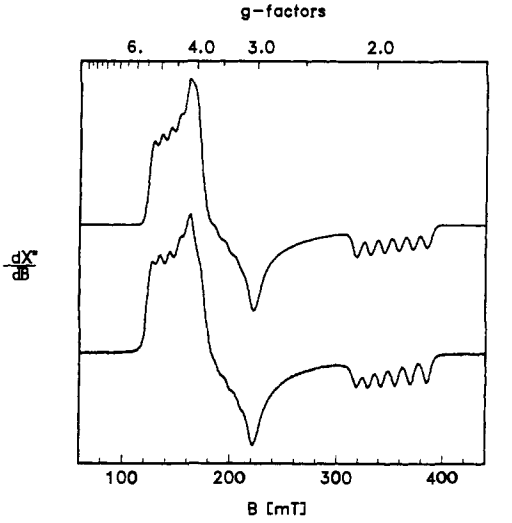

Figure 11. Bottom: Experimental X-band EPR spectrum of a solid sample of $[L'Ru(\mu\text{-}O)(\mu\text{-}CH_3CO_2)_2MnL](BPh_4)_2$ (**4**), recorded at 10 K (microwave frequency = 9.4365 GHz, power = 20 μW). Top: Simulation using $g_i = (3.49, 4.55, 1.915)$, $A_i = (159.7, 176.3, 118) \times 10^{-4}$ cm^{-1}, line width = (5.6, 4.2, 4.5) mT, $i = x, y, z$.

coupling tensor $(153.6, 60.5, 39.4) \times 10^{-4}$ cm^{-1} (Figure 10 top) represents a satisfactory fit of the experimental pattern. A typical vanadyl EPR spectrum is observed in agreement with the assignment of oxidation states in **2** as $[Ru^{II}O V^{IV}]^{2+}$. Similar spectra have been reported for $[(NH_3)_5Ru^{II}(\mu\text{-}O)V^{IV}(Hedta)]^{+}$[37a] in solution at room temperature and for solid $[L'O(H_2O)V^{IV}(\mu\text{-}O)W^{VI}O_2L]Cl(ClO_4)$ at 10 K.[38]

Solid **3** is EPR silent under our experimental conditions as are **5** and **6**. These are integer spin systems where zero-field splitting usually prevents paramagnetic resonances in X-band spectroscopy.

For EPR measurements of the $[RuOMn]^{2+}$ complex **4**, the bis(hexafluorophosphate) salt of **4** was converted to its bis(tetraphenylborate) salt in order to achieve magnetic dilution of the paramagnetic centers in the solid state. This preparation displays a wide, axially split spectrum with significant rhombic distortion and a resolved hyperfine structure (Figure 11). The pattern could be simulated with effective g values $g_x' = 3.49$, $g_y' = 4.55$, $g_z' = 1.915$ and hyperfine interaction with the ^{55}Mn nucleus ($I = {}^5/_2$)

(35) (a) Hudson, A.; Kennedy, M. J. *J. Chem. Soc. (A)* **1969**, 1116. (b) Cotton, F. A.; Torralba, R. C. *Inorg. Chem.* **1991**, *30*, 2196. (c) Cotton, F. A.; Torralba, R. C. *Inorg. Chem.* **1991**, *30*, 4392. (d) Neubold, P.; Della Vedova, S. P. C.; Wieghardt, K.; Nuber, B.; Weiss, J. *Inorg. Chem.* **1990**, *29*, 3355.

(36) Taylor, C. P. S. *Biochem. Biophys. Acta* **1977**, *491*, 137.

(37) Kristine, F. J.; Shepherd, R. E. *Inorg. Chem.* **1978**, *17*, 3145.

(38) Bossek, U.; Knopp, P.; Habenicht, C.; Wieghardt, K.; Nuber, B.; Weiss, J. *J. Chem. Soc., Dalton Trans.* **1991**, 3165.

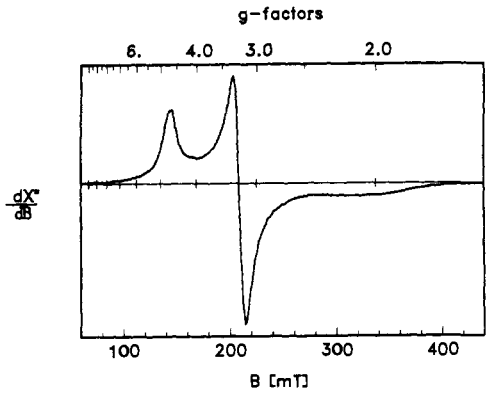

Figure 12. X-band EPR spectrum of a solid sample of **7** at 4.2 K (microwave frequency = 9.4340 GHz; power = 20 μW).

with a hyperfine coupling tensor $A = (176, 160, 118) \times 10^{-4}$ cm^{-1}. Additional interactions with nuclei of ^{99}Ru ($I = {}^3/_2$, 13% natural abundance) and ^{101}Ru ($I = {}^5/_2$, 17% natural abundance) are not resolved but might be a reason for the slight anisotropy of line width, which we had to include in the simulation. Unresolved hyperfine interaction with ^{14}N ligand nuclei could be another source for anisotropic line broadening.

The effective g values of **4** are typical for a well-isolated $|m_s = \pm{}^1/_2\rangle$ Kramers doublet of a spin quartet ($S = {}^3/_2$) with large zero-field splitting ($D \gg h\nu \approx 0.3$ cm^{-1}). The rhombic splitting of the x and y resonances $\Delta g_\perp' = g_y' - g_x' = 1.06$, together with the first-order perturbation expression $\Delta g_\perp'(S={}^3/_2) = 12\,E/D$, yields a rhombicity parameter $E/D = 0.09$. For such a low rhombicity the second Kramers doublet of the quartet is expected to be quasi-EPR silent, in accordance with the measurement.

A comparison of experimental effective g values with theoretical values, obtained from a spin Hamiltonian calculation for the $|S = {}^3/_2, m_s = \pm{}^1/_2\rangle$ doublet with $E/D = 0.09$, allows an estimate of the electronic g values $(g_x + g_y)/2 = 2.01$ and $g_z = 1.97$ for the quartet state of **4**. However, independent determinations of g_x and g_y are not possible without additional spectroscopic data.

As exchange coupling in the Ru–Mn complex **4** is much stronger than zero-field, Zeeman, and hyperfine interactions, the individual spins $S_{Ru} = {}^1/_2$ of Ru(III) and $S_{Mn} = 2$ of Mn(III) may be added vectorially to arrive at the total spin $S = {}^3/_2$ of the ground state. Hence, the g_i and A_i values of the multiplet may be expressed in terms of the local values $g_{i,Ru}$, $g_{i,Mn}$, $A_{i,Mn}$, expected for isolated Ru(III) and Mn(III) ions: $g_i = -{}^1/_5 g_{i,Ru} + {}^6/_5 g_{i,Mn}$, $A_i = {}^6/_5 A_{i,Mn}$, $i = x, y, z$.[39] The rhombicity E/D of the quartet state originates only from manganese (E/D_{Mn}), provided that we can neglect dipolar contributions from anisotropic spin coupling.

If we take the g values (2.18, 2.41, 1.9) of **1** as analogs for those of Ru(III) in **4** we achieve an estimate of Mn(III) parameters in **4**. However, due to the low symmetry of **4**, the relative orientation of principal axes of ligand-field interactions at the Ru and Mn sites are unknown, except that one might speculate that for both ions the z axes point along the bridging μ-oxo ligand. Hence, we can give only ranges of parameters by permuting the Ru values in the above equations: $1.96 \le g_{z,Mn} \le 2.04$, $1.99 \le \langle g_{x,y}\rangle_{Mn} \le 2.08$. The average g values of Mn(III) would be 2.025, for any orientation of axes systems.

In contrast to the g values of Mn(III) in **4**, the determination of the local hyperfine tensor—using the equations from above—is unambiguous. It is $A = (147, 133, 98) \times 10^{-4}$ cm^{-1}, given in the principal axes system of the zero-field interaction (D tensor) of the cluster quartet-spin $S = {}^3/_2$. The anisotropy of A indicates significant orbital contributions to the magnetic moment, in contrast to the findings presented for Mn(III) in mixed valence Mn(II/III) dimers.[40] A preliminary analysis of our g, E/D, and A values, using second-order perturbation expressions for spin-orbital interaction in the $3d^4$ configuration,[41] suggests a d_z ground state, admixed with d_{x-y}, and a splitting of low E_g and excited T_{2g} levels (in distorted octahedral symmetry) of about 10^{+4} cm^{-1}.

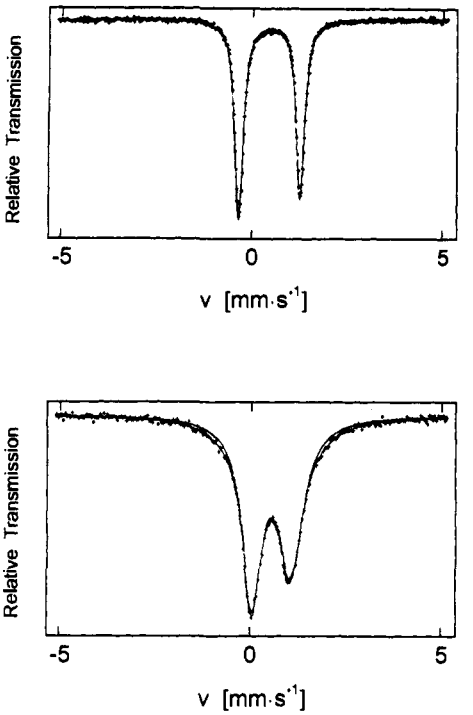

Figure 13. Mössbauer spectrum of **5** at 6 K (top) and of **10** at 290 K (bottom). The solid lines give theoretical simulations using values given in the text.

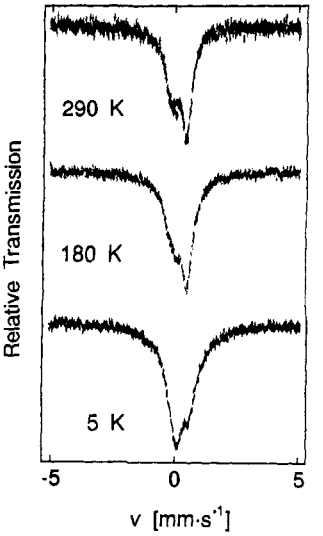

Figure 14. Mössbauer spectrum of **7** at various temperatures.

Figure 12 shows the X-band ESR spectrum of a solid sample of **7** at 4.2 K. Again a typical rhombic signal of a low-symmetry species with an $S = {}^3/_2$ ground state is observed with $g_x = 3.23$, $g_y = 4.7$, and $g_z = 2.05$. No hyperfine splitting is detected. The spectrum corroborates the finding of strong exchange coupling of Ru(IV) ($S = 1$) and Fe(III) ($S = {}^5/_2$) in complex **7**. In terms of local parameters the g values of the dimer spin ($S = {}^3/_2$) are $g_i = -{}^2/_5 g_{i,Ru} + {}^7/_5 g_{i,Ru}$. If we assume an isotropic g tensor $g_i = 2$ for the S-state ion Fe(III), we derive the following for Ru(IV): $\langle g_{x,y}\rangle_{Ru} = 2.05$, $g_{z,Ru} = 1.88$, given in the principal axes system of zero-field interaction.

Mössbauer Spectra. The Mössbauer spectra of $[RuOFe]^{2+}$ (**5**), $[RuOFe]^{3+}$ (**7**), and $[Ru(OH)Fe]^{3+}$ (**10**) were measured at low

(39) Bencini, A.; Gatteschi, D. *EPR of Exchange Coupled Systems*; Springer Verlag; New York, 1990; pp 48–55.

(40) Cooper, S. R.; Dismukes, G. C.; Klein, M. P.; Calvin, M. *J. Am. Chem. Soc.* **1978**, *100*, 7248.

(41) Abragam, A.; Bleaney, B. *Electron Paramagnetic Resonance of Transition Ions*; Dover Publications: New York, 1970.

Table VI. Mössbauer Parameters for Selected Homo- and Heterodinuclear Complexes

complex[b]	T, K	δ,[a] mm s^{-1}	ΔE_Q, mm s^{-1}	ref
$[L'_2Fe^{III}_2O(CH_3CO_2)_2](PF_6)_2$	4.2	0.47 (3)	1.50 (5)	8c
	77	0.47 (3)	1.50 (5)	
$[Fe^{III}_2O(CH_3CO_2)_2(HBpz_3)_2]$	4.2	0.52 (3)	1.60	8d
$[Fe^{III}_2(OH)(CH_3CO_2)_2(HBpz_3)_2](ClO_4)$	80	0.47 (3)	0.25	25
$[L_2Fe^{III}_2O(CH_3CO_2)_2]I_2$	80	0.46 (3)	1.72 (5)	8c
$[L'_2Fe^{II}_2(OH)(CH_3CO_2)_2](ClO_4)$	4.2	1.16 (3)	2.83 (5)	8c
	77	1.15 (3)	2.76 (5)	
$[LFeO(CH_3CO_2)_2RuL'](PF_6)_2$ (**5**)	6.0	0.43	1.60	this work
	78	0.42	1.58	
$[LFe(OH)(CH_3CO_2)_2RuL'](PF_6)_3$ (**10**)	290	0.50	1.06	this work
$[LFeO(CH_3CO_2)_2RuL'](PF_6)_3$ (**7**)	5	0.35	~0.4	this work

[a] Isomer shifts referenced to metallic iron at room temperature. [b] $HBpz_3^-$ represents the hydrotris(pyrazolyl)borate anion; L = 1,4,7-triazacyclononane; L' = 1,4,7-trimethyl-1,4,7-triazacyclononane.

(4.2–8 K), intermediate (~77 K), and higher temperatures (~290 K) in the absence of externally applied magnetic fields. The spectra are shown in Figures 13 and 14. Mössbauer parameters obtained from least-squares fits of the experimental data to Lorentzian line shapes are summarized in Table VI for **5** and **10** and, in addition, for some homodinuclear diiron(III) complexes.

The Mössbauer spectrum of **5** at 6 K (Figure 13) consists of a nearly symmetric quadrupole doublet with an isomer shift of δ = 0.43 (3) mm/s and a quadrupole splitting of ΔE_Q = 1.60 (5) mm/s. The line width (full width at half maximum) of Γ = 0.31 mm/s at 6 K is as in the spectrum of $[L_2Fe_2O(CH_3CO_2)_2](PF_6)_2$.[8c] The isomer shift is well within the range ($0.3 < \delta < 0.6$ mm/s) observed for a wide variety of mononuclear and oxo bridged ferric dinuclear complexes.[42] The large quadrupole splitting is comparable to all oxo bridged homodinuclear 6-coordinate complexes and the met forms of hemerythrin.[42] These results allow unambiguous assignments of the oxidation states in **5** as $[Ru^{III}OFe^{III}]^{2+}$.

The Mössbauer spectrum of the hydroxo bridged species $[Ru(OH)Fe]^{3+}$ (**10**) at 290 K consists of an asymmetric quadrupole doublet with an isomer shift of δ = 0.50 mm/s and a quadrupole splitting of ΔE_Q = 1.06 mm/s ($\Gamma \approx$ 0.80 mm/s).

It is noticed that the isomer shift of **10** is very similar to those observed for **5** and all other homodinuclear ferric complexes[8c] but the quadrupole splitting is smaller in **10** than in **5**. This effect has also been reported for the hydroxo bridged homodinuclear complex $[Fe_2(OH)(CH_3CO_2)_2(HBpz_3)_2](ClO_4)$[25] where $HBpz_3^-$ represents the hydrotris(pyrazolyl)borate anion as compared to its oxo bridged analogue. Protonation of the μ-oxo group causes a significant alteration in the electronic charge distribution at the iron sites, from a highly asymmetric one in the μ-oxo complex to a more spherically symmetrical one in the μ-hydroxo complex.[8c] The Mössbauer spectra at 4.2 K of the heterodinuclear species $[L'Cr(\mu\text{-}O)(\mu\text{-}CH_3CO_2)_2Fe^{III}L](PF_6)_2$ and $[L'Cr(\mu\text{-}OH)(\mu\text{-}CH_3CO_2)_2FeL](PF_6)_3$ with isomer shifts of 0.51 and 0.42 mm/s and quadrupole splittings of 2.02 and 0.49 mm/s, respectively, also show this effect.[43]

The Mössbauer spectrum of $[RuOFe]^{3+}$ (**7**) (Figure 14) differs from those discussed to this point. An asymmetric quadrupole doublet is observed. At 290 K the left absorption line is less intense than the right. At 5 K this behavior is reversed. We have not attempted a Lorentzian fit of these spectra. The isomer shift ($\delta \approx$ 0.35 mm/s at 5 K) appears to be temperature independent and is at the lower limit observed for octahedral high-spin ferric complexes. The quadrupole splitting ($\Delta E_Q \approx$ 0.40 mm/s at 5 K) is significantly smaller than in all other oxo bridged homo- and heterodinuclear ferric species discussed so far: It resembles values found for μ-hydroxo complexes. This is in accord with the results from X-ray crystallography of **7** where it was established that the $Fe\text{–}O_{oxo}$ bond length is significantly longer (1.86 Å) than in all other dinuclear μ-oxo ferric complexes (1.80–1.82 Å). We take this as an indication that the oxo bridge in **7** can be described by the resonance structure $[Ru^{IV}{=}O{-}Fe^{III}]^{3+}$. In summary, although the Mössbauer spectrum of **7** is not understood in all details there is sufficient evidence to support the assignment of oxidation states in **7** as $[Ru^{IV}OFe^{III}]^{3+}$.

Discussion. The present series of complexes allows a detailed study of the bonding in the bent [Ru–O–M] unit. One of the following three resonance structures may represent the bonding in a given $[RuOM]^{2+/3+}$ complex which emphasizes the π-donor capability of the oxo bridge and the π-acceptor capacity of the respective metal ion. In these heterodinuclear complexes M

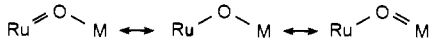

A B C

represents a first-row transition-metal ion. Formation of strong Ru=O and M=O bonds in mononuclear octahedral metal complexes is to a first approximation dependent on the d^n electron configuration of the metal ions.[44] If we assume that the M–O bond in such species coincides with the z-axis and the x- and y-axis are directed along M–L bonds, the d_{xz} and d_{yz} metal orbitals overlap with $p_{x,y}$ orbitals of the oxo ligand forming two π-bonds.[45] In the extreme cases where these d-metal orbitals are either empty (d^0) or fully occupied (d^6 l.s.) an M≡O triple (or M=O double) or only an M—O single bond will be stabilized, respectively. M≡O or M=O bonds are, in general, formed by metal ions with high formal oxidation states and a d^n electron configuration where n ranges from 0 to 5.

The actual oxidation states of the two metal ions in $[RuOM]^{2+}$ and $[RuOM]^{3+}$ species are therefore predominantly determined by the propensity of these metal ions with d^n and d^m electron configurations to form metal-to-oxo double bonds. If we compare the intrinsic stabilities of mononuclear octahedral oxo complexes of Ru(II), Ru(III), and Ru(IV) with those of the first-row transition-metal complexes in their respective oxidation states (M(II), M(III), M(IV)), we should be able to qualitatively obtain an estimate for the most probable distribution of oxidation states in these heterodinuclear complexes. Since we are comparing a first- and second-row transition-metal ion in an identical ligand environment it should be kept in mind that 4d metal orbitals are larger and more diffuse than 3d orbitals and, consequently, the overlap between $4d_{xz}$, $4d_{yz}$ orbitals and p orbitals of the oxo ligand will be more efficient than with $3d_{xz}$, $3d_{yz}$ orbitals.

In $[RuOCo]^{2+}$ (**1**) we consider the possibilities $[Ru^{III}OCo^{III}]^{2+}$, or $[Ru^{II}OCo^{IV}]^{2+}$, or $[Ru^{IV}OCo^{II}]^{2+}$ with low-spin electronic configurations $4d^5\,3d^6$, $4d^6\,3d^5$, $4d^4\,3d^7$ and intuitively assign the resonance structures A, C, and A, respectively. $[Ru^{III}OCo^{III}]^{2+}$ is of course the favored structure because it is very difficult to oxidize Co^{III} to Co^{IV} and octahedral Co^{IV}=O complexes are not known. On the other hand, $[Ru^{IV}OCo^{II}]^{2+}$ with resonance structure A could be a low-lying first excited state (for which we have no experimental evidence). Octahedral Ru^{IV}=O complexes are known and have been structurally characterized.[46] We would

(42) (a) Murray, K. S. *Coord. Chem. Rev.* **1974**, *12*, 1. (b) Gibb, T. C.; Greenwood, N. N. *Mössbauer Spectroscopy*; Chapman and Hall, Ltd.: London, 1971; pp 148–164. (c) Debrunner, P. G. *Hyperfine Interact.* **1990**, *53*, 21.

(43) Debrunner, P. Unpublished results.

(44) Holm, R. H. *Chem. Rev.* **1987**, *87*, 1401.

(45) Nugent, W. A.; Mayer, J. M. *Metal-Ligand Multiple Bonds*; Wiley: New York, 1988.

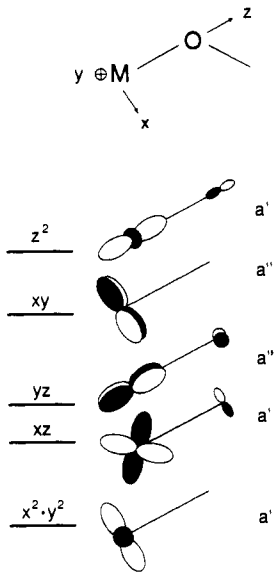

Figure 15. Local magnetic orbitals around one metal ion in the $[RuO(CH_3CO_2)_2M]^{2+/3+}$ unit.

then predict that the oxidized form of **1** is a $[Ru^{IV}OCo^{III}]^{3+}$ species with a structure A.

For $[RuOV]^{2+}$ (**2**) formulations as $[Ru^{III}OV^{III}]^{2+}$, $[Ru^{II}OV^{IV}]^{2+}$, and $[Ru^{IV}OV^{II}]^{2+}$ must be considered. The known stability of octahedral vanadyl complexes with short V=O bonds makes the assignment as $[Ru^{II}OV^{IV}]^{2+}$ attractive. Electrochemically, the $[RuOV]^{3+}$ species is formed at a readily accessible redox potential. We suggest that V(IV) has been oxidized with formation of an octahedral mono-oxovanadium(V) entity, $[Ru^{II}OV^{V}]^{3+}$. In both instances, the V(IV)=O and V(V)=O structures are more stable than Ru^{III}—O or Ru^{IV}=O units in conjunction with V^{III}—O and V^{II}—O units, respectively. Thus the Ru^{II}—O single bond is stabilized due to the inherent stability of V(IV)=O and V(V)=O bonds.

$[RuOCr]^{2+}$ (**3**) is to be formulated as $[Ru^{III}OCr^{III}]^{2+}$ because octahedral Cr^{IV}–O complexes are not known and are probably very strong oxidants whereas high-spin octahedral Cr^{II} complexes are strong reductants in the given ligand environment of these heterodinuclear species. For the same reasons the oxidized form is most probably a $[Ru^{IV}OCr^{III}]^{2+}$ complex.

It is not possible to assign oxidation states in $[RuOMn]^{2+}$ (**4**) and its oxidized form $[RuOMn]^{3+}$ (**6**) using the simple arguments outlined above alone. Their physical properties clearly indicate the presence of $[Ru^{III}OMn^{III}]^{2+}$ in **4** and $[Ru^{III}OMn^{IV}]^{3+}$ in **6**.

For $[RuOFe]^{2+}$ (**5**) and $[RuOFe]^{3+}$ (**7**) the same difficulties prevail but it is noted that octahedral ferryl complexes with an Fe^{IV}=O unit are not known and are probably very strong oxidants.[47] Intuitively, one would favor formulations as $[Ru^{III}OFe^{III}]^{2+}$ and $[Ru^{IV}OFe^{III}]^{3+}$ as have been experimentally verified.

Protonation of μ-oxo groups affording heterodinuclear $[Ru(\mu\text{-}OH)M]^{3+}$ species reduces the π-donor capability of the bridging oxygen atom. As a consequence, the $M\text{–}O_{hydroxo}$ bonds are always weaker than $M\text{–}O_{oxo}$ bonds in complexes where the metal ions have the same oxidation states. This holds only for d^n electron configurations where the d_{xz}, d_{yz} metal orbitals are empty or half-filled by electrons. Secondly, μ-hydroxo bridged complexes stabilize metal ions in lower oxidation states with filled d_{xz} and d_{yz} metal orbitals. Consistent with this notion is the observation that the $[Ru(\mu\text{-}OH)M]^{3+}$ complexes are readily electrochemically reduced with formation of $[Ru(\mu\text{-}OH)M]^{2+}$ species but it is not possible in all cases to predict which of the metal ions act as electron acceptor. The only straightforward case is $[Ru^{II}(\mu\text{-}OH)Cr^{III}]^{2+}$, the reduced form of **9**, as was noted above.

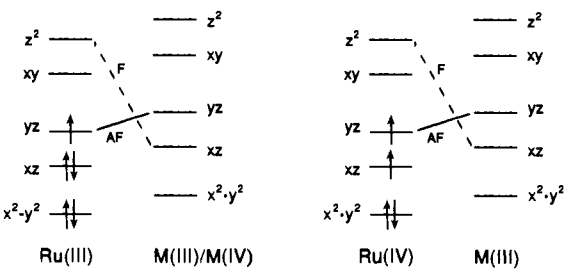

Figure 16. Dominant electron exchange pathways in $[Ru^{III}O(CH_3CO_2)_2M]^{2+/3+}$ (left) and $[Ru^{IV}O(CH_3CO_2)_2M^{III}]^{3+}$ units. Bold lines symbolize antiferromagnetic (AF) while dotted lines stand for ferromagnetic couplings (F).

The magnetic properties of $[RuOM]^{2+}$ and $[RuOM]^{3+}$ species where both metals have unpaired electrons are readily understood by using the model developed recently for heterodinuclear first-row transition-metal complexes containing a (μ-oxo)bis(μ-acetato)-dimetal core.[9] If we consider the following idealized C_{2v} geometry for homodinuclear and—for the sake of simplicity—also for the heterodinuclear complexes we have identified the local magnetic orbitals shown in Figure 15.

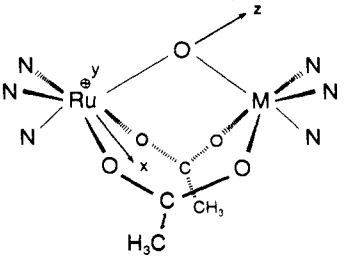

Since both metal ions in the complex have a compressed octahedral geometry, the metal–oxo distance is always the shortest and the corresponding interaction is the strongest. The symmetry at each metal is C_s and the local orbitals are labeled by the irreducible representation of this symmetry group. We have then shown that the largest overlaps between metal d-orbitals and p-orbitals of the oxo group are S_{yz-yz} and the "crossed" interaction S_{z^2-xz}. At small M–O–M angles the $S_{z^2-z^2}$ overlap is small and plays no role in the present series. Thus the two resonance integrals of the leading orbital interactions are β_{yz-yz} and $\beta_{xz-z^2} = \beta_{z^2-xz}$ which will lead to antiferromagnetic interactions J_{yz-yz}^{AF}, $J_{z^2-xz}^{AF}$, and $J_{xz-z^2}^{AF}$ if the d_{z^2}, and d_{yz}, d_{xz} orbitals at both metal ions are half-filled. If, on the other hand, one of these d orbitals at metal 1 is half-filled and the other at metal 2 of a given interaction is empty, a ferromagnetic interaction will prevail (Goodenough–Kanamori rules). As is shown schematically in Figure 16, the β_{yz-yz} interaction provides a dominant antiferromagnetic exchange pathway in all complexes containing a low-spin ruthenium(III) ion and a first-row transition-metal ion with a half-filled d_{yz} orbital: (**3**) $Ru^{III}Cr^{III}$; (**4**) $Ru^{III}Mn^{III}$; (**5**) $Ru^{III}Fe^{III}$; (**6**) $Ru^{III}Mn^{IV}$. This pathway is also available for complexes containing a ruthenium-(IV) ion ($S = 1$) as in **7** ($Ru^{IV}Fe^{III}$). The ferromagnetic contribution from the "crossed" interaction S_{z^2-xz} is obviously much smaller and does not contribute significantly in contrast to the series of homo- and heterodinuclear first-row transition-metal complexes described previously.[9] This is most probably a consequence of the larger energy mismatch of the $3d_{z^2}$ and $4d_{xz}$ metal orbitals of the respective first- and second-row transition-metal ions.

Complexes containing a diamagnetic Ru(II) or Co(III) (d^6 low spin) and a second metal ion with an odd number of d electrons as in **1**, **2**, and **8** display straightforward Curie paramagnetism of the second metal ion (Ru(III), V(IV)).

Protonation of the oxo bridge in these complexes results in a significant lengthening of the ruthenium-to-oxygen and first-row transition-metal ion-to-oxygen bonds in the resulting μ-hydroxo

(46) (a) Yukawa, Y.; Aoyagui, K.; Kurihara, M.; Shirai, K.; Shimizu, K.; Mukaida, M.; Takeuchi, T.; Kakihana, H. *Chem. Lett.* **1985**, 283. (b) Che, C. M.; Wong, K. Y.; Mak, T. C. M. *J. Chem. Soc., Chem. Commun.* **1985**, 546. (c) Che, C. M.; Lai, T. F.; Wong, K.-Y. *Inorg. Chem.* **1987**, *26*, 2289.

(47) Leising, R. A.; Brennan, B. A.; Que, L., Jr.; Fox, B. G.; Münck, E. *J. Am. Chem. Soc.* **1991**, *113*, 3988.

species. This weakens the orbital overlap between the d_{yz} metal and p orbitals of the oxygen and as a consequence the antiferromagnetic coupling decreases in complexes **9** and **10** as compared to their μ-oxo counterparts.

Conclusion

We have developed an efficient synthetic route to oxo and hydroxo bridged, asymmetric, heterodinuclear complexes containing a ruthenium and a first-row transition-metal ion (V, Cr, Mn, Fe). The electronic properties of these complexes were found to be adequately described by using localized oxidation states for both metal ions. Depending on the propensity to form M=O bonds, the ruthenium ion adopts the +II, +III, or even +IV oxidation state. If both metal ions in a given complex have an odd number of d electrons, a very efficient antiferromagnetic superexchange pathway (S_{yz-yz}) couples the spins of the electrons at both metal ions. Protonation of the oxo bridge weakens this pathway significantly.

Acknowledgment. This work was supported by the Deutsche Forschungs-gemeinschaft and the Fonds der Chemischen Industrie. We thank both institutions.

Supplementary Material Available: Lists of atom coordinates, bond distances, bond angles, anisotropic displacement parameters, and calculated positional parameters for hydrogen atoms for complexes **4**, **6**, **7**, and **8** and listings of temperature-dependent susceptibilities of complexes (45 pages); listings of observed and calculated structure amplitudes (72). Ordering information is given on any current mashead page.

Zirconium and Hafnium Polyhydrides. 2. Preparation and Characterization of $M_3H_6(BH_4)_6(PMe_3)_4$ and $M_2H_4(BH_4)_4(dmpe)_2$

John E. Gozum, Scott R. Wilson, and Gregory S. Girolami*

Contribution from the School of Chemical Sciences, The University of Illinois at Urbana—Champaign, 505 South Mathews Avenue, Urbana, Illinois 61801.
Received March 18, 1992

Abstract: Prolonged treatment of the tetrakis(tetrahydroborate) complexes $Zr(BH_4)_4$ or $Hf(BH_4)_4$ with trimethylphosphine has given the first trinuclear group 4 polyhydrides, $M_3H_6(BH_4)_6(PMe_3)_4$, where M is Zr or Hf. The ^1H, ^{31}P, and ^{11}B NMR data suggest that these trinuclear compounds contain noncyclic $M(\mu\text{-}H)_3M(\mu\text{-}H)_3M$ backbones with the phosphine and tetrahydroborate ligands distributed in 2:2:0 and 2:1:3 ratios among the three metal centers. This suggestion has been confirmed by the X-ray crystal structure of $Zr_3H_6(BH_4)_6(PMe_3)_4$. The metal–metal vectors are each bridged by three hydride ligands: the average Zr–H–Zr angle is 108 (2)°, and the Zr···Zr···Zr angle is 124.14 (1)°. The Zr–B distances average 2.633 (4) Å for the η^2-BH_4 groups and 2.368 (6) Å for the η^3-BH_4 groups, while the Zr–P distances average 2.761 (1) Å. The average Zr···Zr distance is 3.164 (1) Å. Interestingly, several of the η^3-BH_4 groups are bonded asymmetrically, so that of the three Zr–H bonds to each BH_4 ligand, one Zr–H bond is longer than the other two. Addition of 1,2-bis(dimethylphosphino)ethane (dmpe) to the previously reported polyhydrides of stoichiometry $M_2H_3(BH_4)_5(PMe_3)_2$ results in phosphine exchange and loss of one BH_3 unit to yield the new dinuclear hydrides $M_2H_4(BH_4)_4(dmpe)_2$. The NMR and X-ray crystallographic data show that three of the hydrides bridge the Zr···Zr axis; the fourth hydride, one η^2-BH_4 group, and the two dmpe ligands are coordinated to one of the zirconium centers, while three asymmetrically-bonded η^3-BH_4 groups are coordinated to the other. The variable-temperature NMR data show that the terminal and bridging hydrides on zirconium exchange with each other via a "windshield wiper" type of motion with an activation energy of 12.6 ± 0.1 kcal mol^{-1}. The X-ray crystal structure of this molecule gives the following distances and angles: Zr···Zr = 3.150 (1) Å, Zr–H_b = 2.03 (8) Å, Zr–H_t = 1.74 (9) Å, Zr–P = 2.715 (3), 2.836 (3) Å, Zr–B = 2.70 (1) Å (η^2-BH_4), Zr–B = 2.39 (2) Å (η^3-BH_4), Zr–H–Zr = 107 (4)°. X-ray data for $C_{12}H_{66}B_6P_4Zr_3$ at 198 K: space group $P2_1/n$, a = 10.142 (5) Å, b = 18.499 (9) Å, c = 19.088 (8) Å, β = 90.49 (4)°, V = 3581 (5) Å^3, Z = 4, R_F = 0.022, and R_{wF} = 0.024 for 426 variables and 4000 unique data for which $I > 2.58\sigma(I)$. X-ray data for $C_{12}H_{52}B_4P_4Zr_2$ at 198 K: space group $Pna2_1$, a = 20.736 (4) Å, b = 9.894 (2) Å, c = 13.788 (4) Å, V = 2829 (2) Å^3, Z = 4, R_F = 0.046, and R_{wF} = 0.036 for 241 variables and 1965 unique data for which $I > 2.58\sigma(I)$.

Introduction

Compounds that contain direct metal–hydrogen bonds are of great interest due to the large number of stoichiometric and catalytic processes in which they are implicated.[1-3] Hydrides of the late transition metals are particularly active in these respects, and thus they have been studied extensively; in contrast, the chemistry of early transition metal hydrides remains largely unexplored, and polyhydrides of the early transition elements are particularly rare.[4-6] Although transition metal hydrides have traditionally been of interest due to their catalytic activity, they may also be involved in certain chemical vapor deposition processes for the growth of thin films that contain transition metals. Many CVD procedures employ H_2 as a carrier gas, and it is possible that in some cases transition metal hydrides are formed as intermediates that subsequently lose H_2 by reductive elimination.

(1) Muetterties, E. L. *Transition Metal Hydrides*; Marcel Dekker: New York, 1967.
(2) Bau, R. *Transition Metal Hydrides*, Advances in Chemistry Series 167; American Chemical Society: Washington, DC, 1978.
(3) Kaesz, H. D.; Saillant, R. B. *Chem. Rev.* **1972**, *72*, 231-281.
(4) Toogood, G. E.; Wallbridge, M. G. H. *Adv. Inorg. Chem. Radiochem.* **1982**, *25*, 267-340.
(5) For Part 1 of this series, see: Gozum, J. E.; Girolami, G. S. *J. Am. Chem. Soc.* **1991**, *113*, 3829-3837.
(6) For the present discussion, polyhydrides will be defined as coordination complexes that contain more than one hydride per metal center.

0002-7863/92/1514-9483$03.00/0